Universidade de Aveiro
2007

Departamento de
Electrónica, Telecomunicações e Informática

Rui Manuel Estanqueiro Santos

Impacto da Distorção não Linear em Sistemas Sem Fios

Universidade de Aveiro
2007

Departamento de
Electrónica, Telecomunicações e Informática

Rui Manuel Estanqueiro Santos

Impacto da Distorção não Linear em Sistemas Wireless

dissertação apresentada à Universidade de Aveiro para cumprimento dos requisitos necessários à obtenção do grau de Mestre em Electrónica e Telecomunicações, realizada sob a orientação científica do Dr. Nuno Borges Carvalho, Professor associado do Departamento de Electrónica, Telecomunicações e Informática da Universidade de Aveiro

o júri

presidente

Prof. Dr. José Carlos Pedro
professor Catedrático da Universidade de Aveiro

Prof. Dr. Paulo Jorge dos Santos Gonçalves Ferreira
professor Catedrático da Universidade de Aveiro

Prof. Dr. Nuno Borges Carvalho
professor associado da Universidade de Aveiro

Agradecimentos

Gostaria de agradacer ao meu orientador Prof. Dr. Nuno Borges Carvalho pelo apoio, motivação e colaboração. Gostava também de gradecer ao Prof. Antonio Caetano pela disponibilidade.

palavras-chave Amplificador de Potência, EVM, Distorção, SNR.

resumo

Esta tese esta inserida no domínio dos sistemas não lineares sendo direccionada para sistemas de micro ondas e radio frequência. Neste estudo pretende-se compreender o impacto da distorção não linear em sistemas wireless quando submetidos a sinais digitais modulados.

Para fazer o estudo destes fenomenos é necessario efectuar uma correcta carcterização do sinal de excitação, contudo devido á sua natureza aleatoria este processo nem sempre é facil, o que originou simplificações, que no entanto são por vezes aplicadas de modo errado. Neste estudo é aboradado este problema sendo ilustradas as diferenças entre as aproximações e a estatistica real do sinal e ainda exposto o processo para o calculo analitico da estatistica real do sinal.

Serão também estudados diversos fenomenos responsaveis pelo aparecimento de distorção não linear, estes fenomenos serão representados através de modelos, tais como, o modelo de Winner-Hammerstein e o modelo multi-slice.

keywords Power Amplifier, EVM, Distortion, SNR

abstract

This thesis is performed under the non-linear electronic systems context, as radio frequency and microwave systems, this study is intended for the understanding of the impact of the non linear distortion in wireless systems when using complex digitally modulated signals.

To evaluate it is necessary to make a correct characterization of the excitation signal. However, due to its random nature, these processes are not always easy, which leads to simplifications. Although this simplifications sometimes are used wrongly.

These will be discussed and the differences between the real signal statistics and the approximations will be showed, moreover the analytical process to obtain the real signal statistics will be presented.

Several non linear phenomena responsible for the non linear distortion will be studied. Each component will be represented by models as the Wiener-Hammerstein and the multi-slice model.

Table of Contents

List of Figures

Chapter 1

1 Introduction

1.1 Wireless Systems

The use of wireless systems started with the analogue radio, using Frequency modulation, FM, and amplitude modulation, AM, techniques when the spectrum limitation was not a problem and the bit rates were reduced. Later, digital modulation schemes, [1], were proposed, which brought security, high data bit rates, communication quality, spectral efficiency and a decrease in the bit error rate.

However, around ten years ago, a massive evolution of wireless devices were introduced on a commercial level, and since then, our lifestyles have irreversibly changed. This is so significant that we cannot imagine our life without mobile services, these being the most important example: GSM, the European standard and IS-95, the American standard.

The reduced costs, the almost one hundred per cent connectivity, the full mobility and the high voice quality service allowed 2G systems to have a penetration tax above one hundred per cent which turned it, into one of the biggest commercial successes ever. This created great expectations for all wireless companies and as a result, an intensive field of research was generated to offer new services with hopes of creating the same commercial success as the 2G systems. The objective was to develop mobile devices able to offer more demanding services than voice, this effort was known as 3G. The most popular 3G systems are WCDMA and CDMA2000 [2, 3], these try to offer multimedia services while maintaining full mobility. To achieve this objective the main upgrade in relation to the 2G systems was the use of the CDMA technique in the

European case and also the rake receiver [4] which can reduce the fading effects originated by the increase of bandwidth. Although was proved that 3G systems could not follow the expectations. Nowadays, the telecommunications market is waiting for promising wireless systems able to reach data rates near of 50 Mbits/s with high mobility, and most of all a system that fulfil the expectations created by the 3G systems.

In the last few years we have witnessed the enormous growth of wireless systems, simultaneous with that, the Bandwidth necessary was also increased by channel. As a result of this phenomenon, the limited available spectrum was quickly occupied becoming a precious resource. Currently some alternatives are in discussion to overcome this issue one of which is the cognitive radio technology [6].

Therefore several changes in wireless architectures have been made, for example: a reduction of the guard band between adjacent channels, new complex modulation techniques were introduced mixing amplitude modulation with phase modulation. Simultaneously the amplifier operation point was moved to the saturation in order to get the better trade-off between power and. efficiency. These changes increase the distortion level at the and consequently decrease the Signal to Noise Ratio, SNR, this reduction comes both from their own channel as well as the adjacent channels interference, therefore the tolerance margin for the system behaviour prediction will be reduced and more accurate analysis has to be done.

These changes required more demanding designs of the wireless systems specifically in the Power Amplifier. Effects until now, unknown or neglected, start to play an important role in the overall system performance, moreover all analysis made must be redesigned in order to accommodate these new effects. Several approximations to characterize the RF signal (Gaussian assumption) as well as the models used to describe de PA behaviour (memoryless) are no longer accurate as the system engineers needs to correctly project wireless systems which have less tolerance margins, therefore new efforts must be made to make a precise prediction of systems behaviour and also powerful simulation tools must be available to carry on this task.

1.2 Dissertation Overview

This Dissertation is divided in six parts, in the first chapter some general concepts are introduced associated to the system level analysis, which are used along this dissertation. In Chapter 3 we explain the statistic nature of the RF digitally modulated signals and methods used to represent it. In Chapter 4 we give a step further studying new nonlinear phenomena in Power Amplifiers, to quantify them we use the figure of merit EVM. To confirm the results previous obtained we perform simulations in Chapter 5. To complete the previous chapter, Chapter 6 presents some measures showing the real behavior of memory effects when real signals are used. At last, Chapter 7 presents conclusions and suggestions for future work.
During the elaboration of this thesis the follow contributions were made:

[1] Rui M. Estanqueiro Santos, N. B. Carvalho and Kevin Gard, “Degradation of CDMA Wireless Communications due to PA Nonlinearities Presenting Long Term Memory Effects” submitted to Microwave Transactions and Techniques

[2] Rui M. Estanqueiro Santos, N. B. Carvalho and “EVM estimation in RF/Wireless Components” submitted to PIMRC. Athens, 2007.

[3] Rui M. Estanqueiro Santos, N. B. Carvalho and Kevin Gard, “The Impact of Long Term Memory Effects in Wireless QPSK Modulated Signals”, in IEEE MTT-S International Microwave Symposium, Hawaii 2007

[4] Rui M. Estanqueiro Santos, N. B. Carvalho and “System Figures of merit Evaluation in Non-linear Amplification of Digitally modulated Signals” in Confetele. Peniche, 2007.

[5] Rui M. Estanqueiro Santos, N. B. Carvalho and João P. Martins, “Envelope Time Trajectories of Multi-sine Signals" in INMMIC Conference. Aveiro, 2006.

Chapter 2

2 System Level Concepts

In this section a brief explanation of the main concepts related with the system level analysis point of view are presented. The signal envelope concept, as well as the mathematical definition is defined. Some aspects associated with distortion characteristics are introduced. Since the system level analysis is mainly based on simulation, the simulation procedures are explained. Moreover, two essential figures of merit for the system level analysis and therefore for the system characterization are introduced.

2.1 Signal Envelope Definition

The wireless signals are commonly generated using a quadrature modulator as shown in Fig. 1. The digital information is divided in two branches, in each one the digital information is filtered with a pulse shaping filter and up-converted orthogonally to the carrier frequency, being then summed to form the modulated carrier, in Fig. 2, we can see the signal evolution in the time domain at each point of the modulator.

The mathematical definition of complex envelope of a amplitude and phase modulated carrier *v(t)* with f_c the carrier frequency, is given by:

$$v(t) = A(t)\cdot\cos(\omega_c \cdot t + \theta(t)) = \frac{1}{2}\cdot\tilde{c}(t)\cdot e^{j\cdot\omega_c\cdot t} + \frac{1}{2}\cdot\tilde{c}^*(t)\cdot e^{-j\cdot\omega_c\cdot t} \qquad \textit{Eq 2-1}$$

With the complex envelope:

$$\tilde{c}(t) = i(t) + j \cdot q(t) \qquad \textit{Eq 2-2}$$

where *i(t)* and *q(t)* being the pulse shaped in-phase and quadrature components and $\omega_c = 2\pi f_c$ and*:*

$$A(t) = \sqrt{i^2(t) + q^2(t)}$$

$$\theta(t) = \tan^{-1}\left(\frac{q^2(t)}{i^2(t)}\right)$$

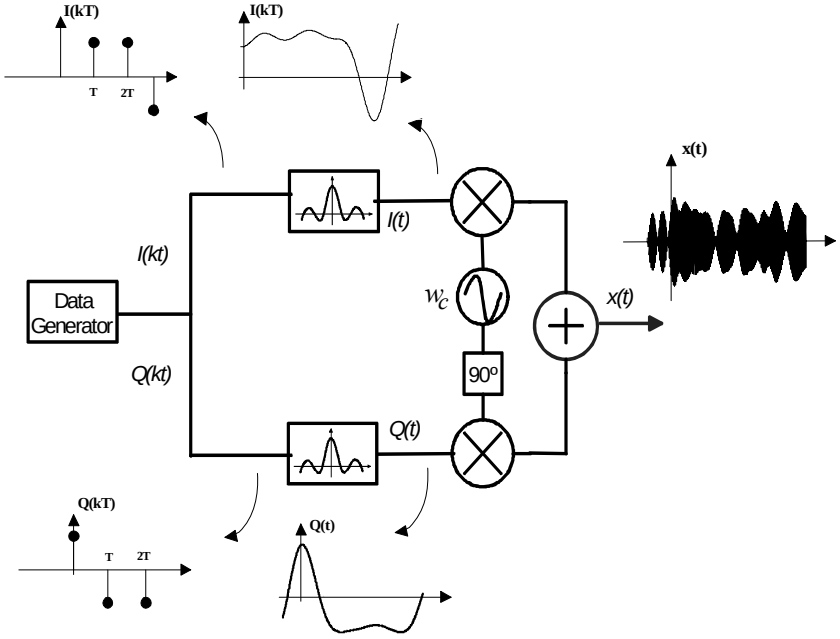

Fig. 1 - I/Q Modulator

There are two types of complex envelopes, constant and non-constant envelopes. Systems without amplitude modulation have constant envelope (QPSK, GMSK) otherwise systems with amplitude modulation have non-constant envelopes (16-QAM). The envelope variations cause a decrease in the PA efficiency, due to the needed of a

backoff factor, to prevent the peaks in the signal to excite the nonlinearities. These peaks can excite the nonlinear behaviour of the PA and consequently increase the distortion at the co-channel as well as at the adjacent channel which decrease the SNR, both in their own channel as in the adjacent channels communications respectively.

This phenomena is often known as intermodulation distortion, IMD, which is observed for digitally modulated signals through the spectral regrowth or the adjacent channel distortion.

However to increase the throughput is necessary to use modulations which present envelope variations, therefore a tradeoff between envelope variations and PA efficiency should be obtained.

Nevertheless it is interesting to note that even QPSK signals present variations in its envelope due to the baseband filtering processes as shows in Fig. 2, these variations will be more severe in the direct link case where there are several users sharing the same channel and the envelope variations will increase as the number of users increase. In Fig. 2 the time domain waveforms are presented corresponding to the branches of the I/Q modulator presented on Fig. 1.

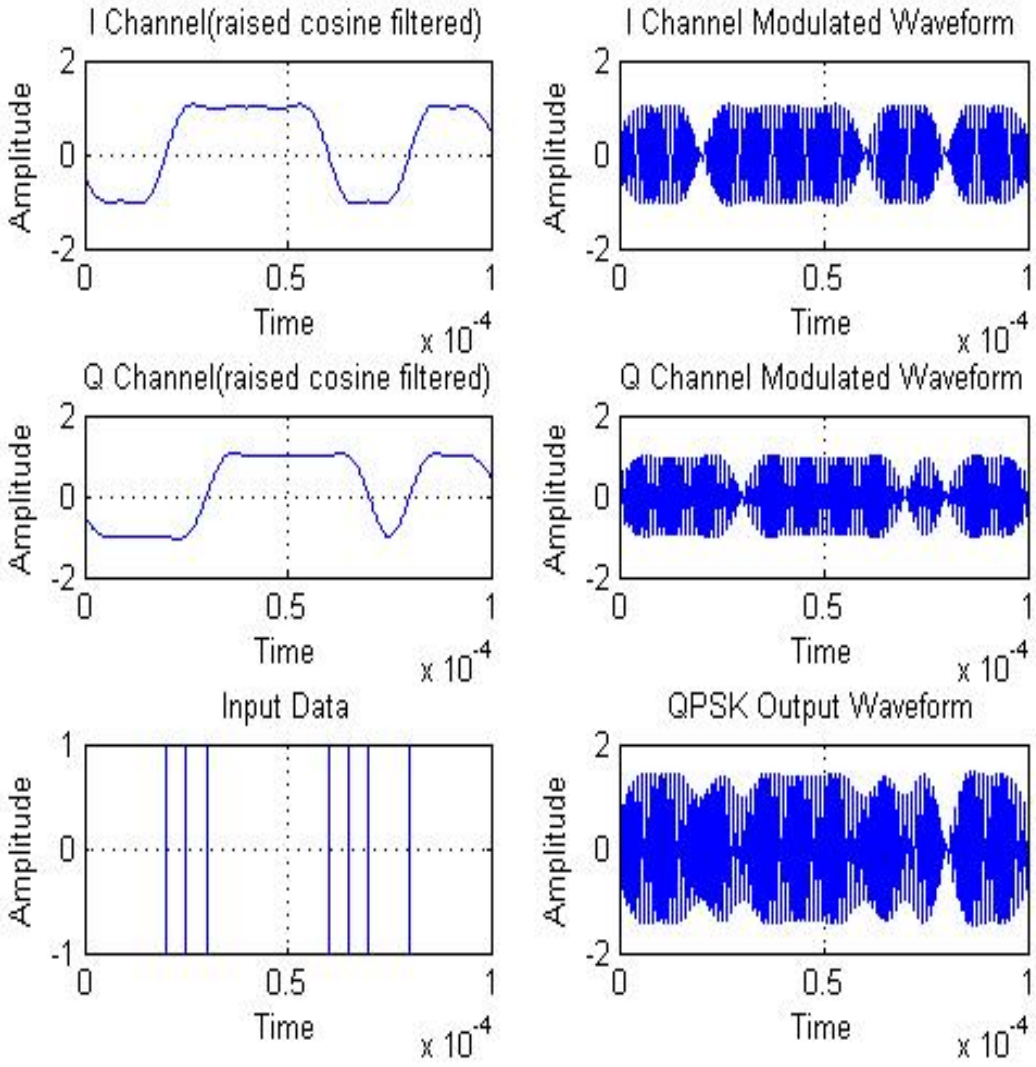

Fig. 2 - QPSK time waveforms

2.2 Spectral Regrowth

When a digitally modulated signal passes through a nonlinear wireless circuit, not only co-channel distortion is generated, but also adjacent channel distortion on both sides of the carrier, this is often called as spectral regrowth.

Spectral regrowth becomes more important as amplitude modulated signals starts to be used with higher M for M-QAM modulations, these cause large envelope variations which will increase the spectral regrowth. This becomes even more important as the

band guard between adjacent channels is reduced due to the limited spectrum.

Another problem, that arises due to spectral regrowth is the cross-modulation in the receivers duplex. The isolation between the transmitter and receiver ports is not infinite and in presence of a strong in-band jammer the receiver can be affected by the jammer spectrum due to the convolution process between the transmitted spectral regrowth and the jammer. This phenomena was thoroughly studied on [8].

So its very important to understand the origin of the envelope variations and how it is related to the system's parameters in order to make the implementation of linearization techniques.

A usual form to quantify the interference caused by a channel on the adjacent channels is through the figure of merit, Adjacent Channel Power Ratio, ACPR.

ACPR has several definitions and can be performed in the upper and lower adjacent spectrum, (2-3) presents the definition for the total ACPR.

$$ACPR = \frac{\int_{f2}^{f3} S_{co}(f)\, df}{\int_{f1}^{f2} S_{L\_ad}(f)\, df + \int_{f1}^{f2} S_{H\_ad}(f)\, df} \qquad \textit{Eq 2-3}$$

With f_2 and f_3 the co-channel spectrum limits, f_1 and f_2 the the low adjacent channel spectrum limits spectrum and f_3 and f_4 the high adjacent channel spectrum limits. S_{co} is the amplitude of the co-channel spectrum and S_{L_ad} and S_{H_ad} the amplitude of the low and high adjacent channels spectrum respectively.

2.3 Error Vector Magnitude

The possible relations between EVM and RF/Wireless components figures of merit is of primordial importance for improving the system specifications between the RF circuit design engineer and the RF/Wireless system design engineer.

The understanding of these relationships allows the RF circuit design to be able to

make some compromises without sacrificing the system behavior of the overall scenario. This is why there are several papers that deal with this problem in the past, by allowing a precise study of the relation between typical figures of merit of RF devices as Intercept point of third order, IP3, phase noise, noise figure, etc and EVM.

The most important relation established with EVM is with SNR, which is the principle figure of merit for any electronic system and is given by:

$$EVM = \frac{1}{\sqrt{SNR}} \qquad \text{Eq 2-4}$$

Expression (2-4) its as, or even more important having in mind (2-5) where we can relate SNR with the system distortion level, S_{uncorr}:

$$SNR = \frac{S_{corr}}{S_{uncorr}} \qquad \text{Eq 2-5}$$

Where S_{corr} and S_{uncorr} are the correlated and uncorrelated parts of the spectrum respectively.

EVM is a figure of merit that quantifies the quality of digital modulated signals, and is defined by the following formula:

$$EVM = \sqrt{\frac{\sum_{n=-\infty}^{+\infty}\left[\left(X_i(nT)-x_i(nT)\right)^2+\left(X_q(nT)-x_q(nT)\right)^2\right]}{\sum_{n=-\infty}^{+\infty}\left[X_i^2(nT)+X_q^2(nT)\right]}} \qquad \text{Eq 2-6}$$

Where (X_i,X_q) are the ideal in-phase and quadrature components respectively, (x_i,x_q) are the correspondent optimal output sampling position measured values, and T the bit period. EVM is a figure of merit which is signal independent, therefore its blind to baseband pulse shaping format, envelope variations or even pre-distortion mechanisms. This is so because it only quantifies the optimal demodulated sampling moments.

EVM can be increased due to amplitude and phase changes originated by linear

and nonlinear phenomena, although linear deviations can be viewed as power scales.

EVM is the mean of the total power deviation, in cases where the system do not introduce band limitations all symbols will suffer the same effects independently of the bit sequence, thus every symbol has the same deviation, obviously propositional to its complex envelope power [21]. In this case the deviation to the ideal constellation is only due to distortion, and so EVM will be a good measure of the system distortion, through expressions (2-4) and consequently (2-5).

In the above condition we only have to calculate each different constellation symbol for the entire observation interval once. The symbols that have different complex power envelopes are considered different symbols.

Looking briefly to (2-6) and remembering the definition of a complex power[1] envelope signal for one symbol:

$$\widetilde{P}_{in} = X_i^2 + X_q^2 \qquad \text{Eq 2-7}$$

Where the tilde is used to indicate the complex envelope format.

Expression (2-6) can be seen as the square root of the normalized power deviation from each measured symbol to the equivalent ideal symbol. The relation between the vector distance and the difference of two complex envelope power signals is given by:

$$vector = \sqrt{(X_i - x_i)^2 + (X_q - x_q)^2} = \sqrt{\widetilde{P}_{error}} \qquad \text{Eq 2-8}$$

Where

$$\sqrt{\widetilde{P}_{in}} = \sqrt{X_i{}^2 + X_q{}^2} \qquad \text{Eq 2-9}$$

$$\sqrt{\widetilde{P}_{out}} = \sqrt{x_i{}^2 + x_q{}^2}$$

[1] We consider that X_i uncorrelated with X_q

We can represent this on Fig. 3.

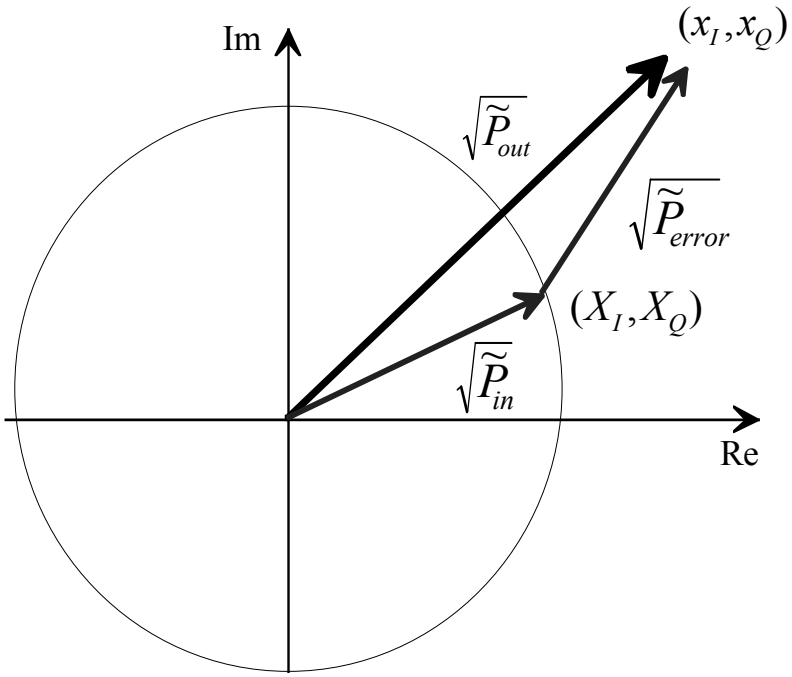

Fig. 3 - EVM Vector Representation

So (2-6) can be rewritten as follows:

$$EVM = \frac{\left|\sqrt{\widetilde{P}_{out}} - \sqrt{\widetilde{P}_{in}}\right|}{\sqrt{\widetilde{P}_{in}}} = \frac{\sqrt{\widetilde{P}_{error}}}{\sqrt{\widetilde{P}_{in}}} \qquad \text{Eq 2-10}$$

Expression (2-10) is valid only for systems which don't introduce phase shift in the constellation, thus this approach is valid only for systems that preserve the phase of the input complex envelope signals, like memoryless devices which only consider amplitude variations for $\sqrt{\widetilde{P}_{out}}$ along the $\sqrt{\widetilde{P}_{in}}$ vector direction. Fig. 3 demonstrates a system which introduces phase changes, therefore (2-10) is no longer valid. This problem will be dealt with in the section where the model WH model is considered.

2.4 Peak to Average Power Ratio

In the wireless systems, the Peak to Average Power Ratio, PAPR, starts to be an intensive object of study since the introduction of the CDMA technology, where several users share the same time and spectrum which associated with non constant envelope modulations even using modulation formats as QPSK/OQPSK[2] leads to larges envelope variations which will decrease the PA efficiency.
PAPR is defined in (2-11).

$$PAPR = 10 \cdot Log_{10}\left(\frac{P_{\max}}{P_{av}}\right) \qquad Eq\ 2\text{-}11$$

Where P_{max} is the maximum power and P_{av} the average power of the signal envelope. Although PAPR is not a helpful tool to characterize the system performance by its own. As an example in certain cases a signal with an higher PAPR can present less distortion than a signal with a lower PAPR, which seems contradictory, however this is due to the frequency of how peaks occur, and also depends on the observation interval, so it is very important to characterize the frequency of how the peaks occur, in other words, if a maximum peak occurs once in a long time we do not need to project a PA obey the IMD for that peak. Instead we must establish a value of a peak probability density funcyion. Therefore the introduction of another system figure of merit is clear, Instantaneous to Average Power Ratio, IAR.

$$IAR = \frac{P(t)}{P_{av}} \qquad Eq\ 2\text{-}12$$

Which gives the ratio of the signal envelope above the mean value, and to obtain a certain probability of power peak, *x*, we use (2-13):

[2] these signals lose the constant envelope property due to the baseband filtering process

$$\Pr\{IAR > x\} \qquad \textit{Eq 2-13}$$

By usually standards, several efforts have been made to reduce the PAPR issue. In CDMA2000 and WCDMA the Hybrid Shift Keying, HPSK, was introduced consisting of a more efficient use of the chip codes, using a process called complex scrambling, the zero crossing and the 0^o shifts are reduced. For instance, with this technique the PAPR was improved by 1.5 dB in relation to IS-95, which uses a simple chip scramble, the scheme is represented in Fig. 4.

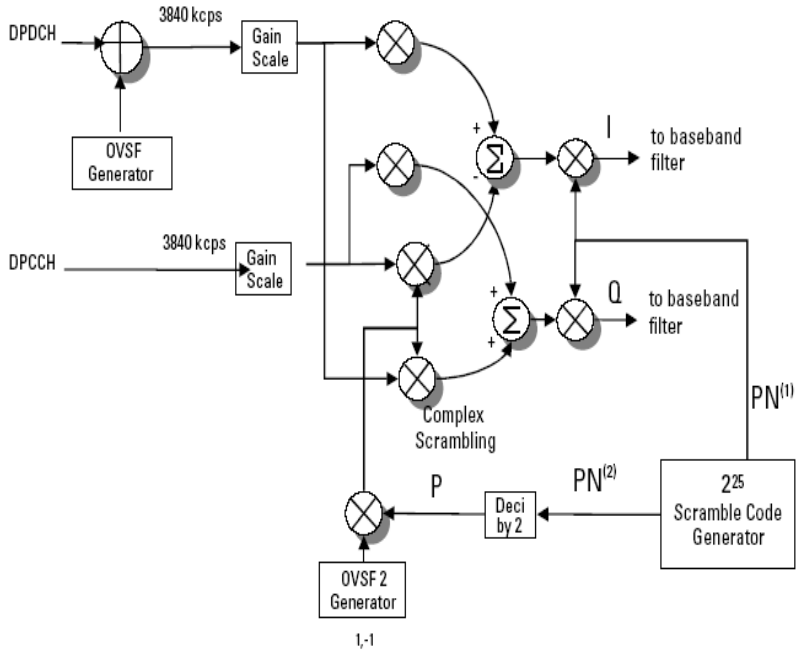

Fig. 4 - WCDMA reverse link[3]

With this method, only a pre defined chip sequences are used which reduce the set of available sequences. This occurs at the scrambling code level as Walsh codes, the PN sequence do not suffer any change and it is the same for both I/Q path's.

Another interesting observation was performed in [22] showing that do not exist a direct relation between peak average ratio, PAPR, and distortion. They also saw that a QPSK modulation have a higher PAPR than a OQPSK, although a QPSK signal

[3] Picture tacken from [58]

exhibits a lower spectral regrowth.

Beyond the intrinsic PAPR reducing techniques explained above, several other techniques has been proposed along the times, schemes as active constellation extension [23, 26], tone injection [27, 28], tone reservation [29, 32], amplitude clipping [33-38], companding techniques [39-43], and mixing techniques are used.

2.5 Simulation Method

CAD/CAE techniques are fundamental to allow the design engineers to simulate wireless systems and to predict the overall system response at the RF frequency. Nowadays, with the use of complex modulation schemes, as well as higher RF carriers, the sample period must be higher and the time steps must be smaller in order to get a valid sampling capable of mimicking the real signal. However it will take a enormous amount of time to simulate as well as to generate an enormous set of values which are hard to handle reducing the utility of the simulation process. So it becomes essential to have an efficient simulation tool that optimize this type simulation.

The circuit Envelope simulation [7] is a very efficient tool which combines time-domain with frequency-domain techniques, where the input is a time-varying amplitude and phase modulation (i.e. complex envelope) RF carrier.

To reduce the number of points, and consequently the time simulation, the signal around the carrier is transferred to DC and all analysis is done with the base band signal version (complex envelope). To do this, the simulator will take samples of the RF signal with a minimum frequency *2BW* where *BW* is the base band signal bandwidth in accordance with the sampling theorem. This is done in all harmonics that result from the non-linear system under analysis. In Fig. 5 a visual representation of this complex envelope simulation method is presented.

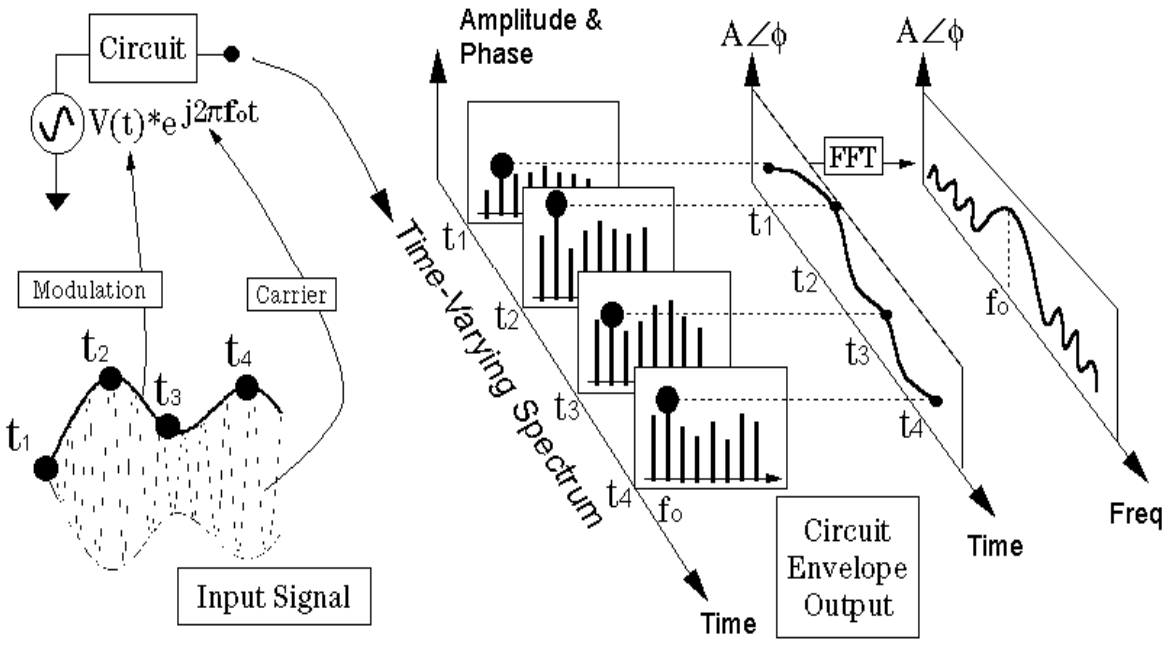

Fig. 5 - Schematic envelope simulation principle[4]

2.6 System level analysis

As the CDMA signal is a time-varying envelope, it is very affected by the odd order PA nonlinearities, through the spectrum spreading around carrier generating intermodulation distortion both co-channel and adjacent channel.

In order to obtain an analytical solution, a behavioural model has been developed, both at the circuit level as well as at the system level, in order to analyze the distortion at the output of a nonlinear amplifier driven by a digitally modulated signal. An accurate analysis depends on the models precision as well as the knowledge of the CDMA signal statistics.

At this level the analysis is based on models and approximations, as a result accurate models and approximations for the system level are primordial to a correct system design. The predictions of the system's behaviour and the adjustments made to its design are done according to that analysis, usually performed in the spectrum

[4] Picture taken from [59].

domain.

To characterize the distortion generated by a digitally modulated signal passed through a nonlinear RF circuit, two main contributions were made: one by Gard [11] and another by Aparin [13]. Both obtained closed forms able to separate the response in several components, correlated and uncorrelated parts.

First [11] estimate an analytical expression for the output power spectrum when the nonlinear circuit is modelled by a complex power series, however he assume the RF digitally modulated signal as being Gaussian. This greatly simplifies the problem due to the well known Gaussian statistical properties, however this simplification is only verified in multi-carrier signals and in the direct link mode were a large number of Walsh-coded channels are transmitted simultaneously resulting in a normal distribution according the central limit theorem. Nevertheless a signal transmitted by a mobile station, where only a single channel is transmitted, has a very distinct behaviour from the narrow band Gaussian noise, NBGB leading to distinct estimates.

The author of [12] recognizes the distinct behaviour between a QPSK and a NBGN process, computing the higher order moments numerically.

Afterwards, Aparin [13] obtained closed form expressions for QPSK and OQPSK modulations in a IS-94 and IS-95 reverse link systems respectively, using the real signal statistics.

He also calculated the uncorrelated part of the spectrum for both the co-channel and adjacent channel which is responsible for the distortion phenomena. This result is obtained based on [14] and where a excellent mathematical work was done obtaining closed form expressions for the higher joint order moments of the base band pulse shaped signals, with the same format as the CMDA IS-95 signals.

The rise of the RF bandwidth brought new phenomena which are usually known as long term memory effects. Several scientific works have been done on this scenario, and the theme is nowadays commonly studied [15-17]. A deep study of this type of scheme can be found in [15] and [18]. Some authors have tried to represent these memory effects using some special behavioural models [19], which somehow represent the mechanism that was already described. This model has already proven to be as accurate as the real effects of the long term memory behaviour as shown in [19] presenting quite good results when applied to a PA presenting memory effects, coming

from the bias networks [20]. Several works have been done, in this field although most of them were made using the two tone test [15] or multi-sine signals [20] but a study with real signals was not done yet.

Chapter 3

3 Modulated Communications Signal Statistics

The efforts above described, should be supported by a strong statistical framework for a correct prevision of the system behaviour when passing through a nonlinearity. Due to the random nature of RF signals, it is necessary to use a statistic model to handle and analyze the signals. Unfortunately the statistical property's of these signals are difficult to obtain in an analytical form. So, to overcome this issue, behavioural techniques are applied under certain restrictions.

In this chapter the most used statistic process to represent Narrow Band RF signals, the Gaussian approximation will be used. Furthermore some methods to obtain the analytical solution for any order of an M-QAM CDMA signal moments will also be addressed.

3.1 Signal Statistics

Statistics are an essential tool to make analytical analysis of the systems' behaviours due to the random nature of the digital information generated in the transmitter, consequently, all analysis are based on the signal's statistics, so the knowledge of the real signal statistic is essential to predict a correct system behaviour.

In order to simplify the system analysis, several simplifications have been made to model the signal statistics [9], however, these simplifications can be applied only under certain conditions.

One of the most used statistic simplifications represents the RF digitally modulated signal by a Gaussian process. With the properties obtained by [10] some simplifications can be done for Gaussian processes, turning this calculation straightforward.

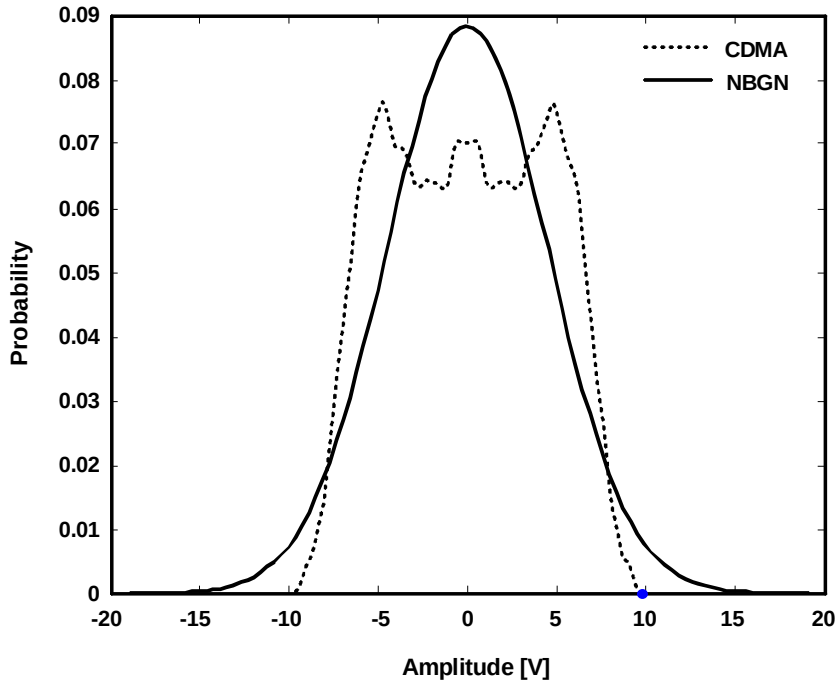

Fig. 6 - Probability Density Function, pdf, of a CDMA and NBGN

The difference between a Gaussian process and the real CDMA statistic for a reverse-link mode can be viewed in Fig. 6, through the probability density function, PDF.
In the past this was used without question. Aparin then predicted the correct statistics for a QPSK signal, however the calculation for a M-QAM remains undiscovered.

The Gaussian assumption, is currently used when analysing systems such as a direct link 3G systems, OFDM WLAN and multiple code channel CDMA/WCDMA systems, mainly due to the large number theory. Fig. 7 presents the spectrum mask for one and sixteen users, Fig. 7.a and Fig. 7.b respectively. A large difference is clearly seen in these figures on the uncorrelated distortion curve (green trace) for both the co-channel and the adjacent channel (spectral regrowth).

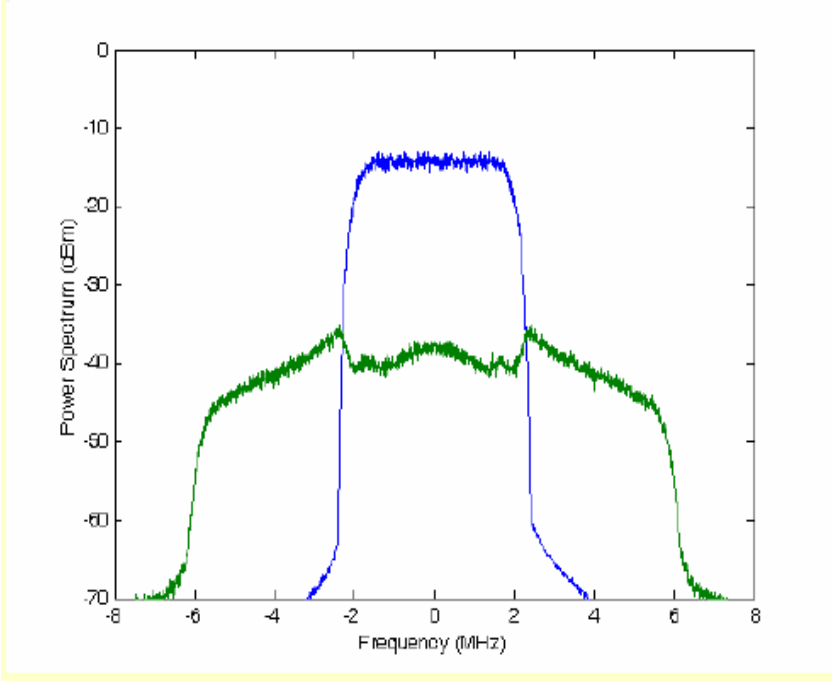

a)

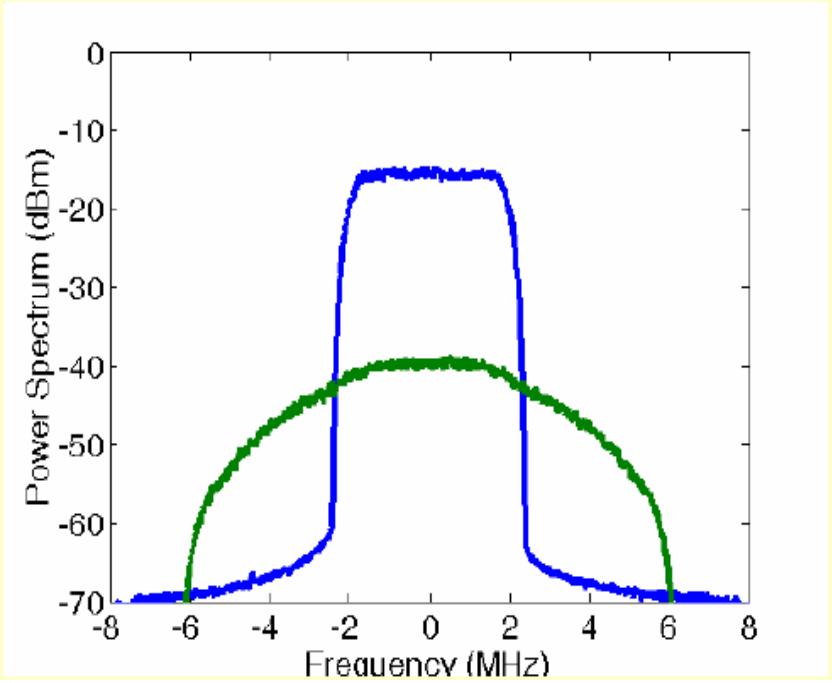

b)

Fig. 7 – Correlated and uncorrelated spectrum for a IS-95 a) 1 user b) 16 users[5]

[5] Picture taken from [60]

This proves the necessity for obtaining the correct statistic of the RF signals, in order to make a correct analysis of the system behaviour.

We must also have in mind that the number of users sharing the same PA is generally reduced in a CDMA system. This fact, and of course the reverse link case where we just have one user, implies a distinct behaviour from the Gaussian process approach.

3.2 Gaussian Process

The most used statistic model is the Gaussian approach, based on the central limit theorem, which states that the sum of independent random variables tends towards a Gaussian distribution with increasing number of variables. This property allows the follow simplifications [10]:

$$E\left[\tilde{z}_1\tilde{z}_2\tilde{z}_3^*\tilde{z}_4^*\right] = E\left[\tilde{z}_1\tilde{z}_3^*\right]\cdot E\left[\tilde{z}_2\tilde{z}_4^*\right] + E\left[\tilde{z}_2\tilde{z}_3^*\right]\cdot E\left[\tilde{z}_1\tilde{z}_4^*\right] \qquad \textit{Eq 3-1}$$

and

$$E\left[\left(\tilde{z}_1\tilde{z}_2^*\right)^n\right] = n!\,E\left[\tilde{z}_1\tilde{z}_2^*\right]^n = n!\,\tilde{R}_{zz}^n(\tau) \qquad \textit{Eq 3-2}$$

Where $\tilde{z}(t)$ is the complex envelope of the quadrature RF digitally modulated signal, and $\tilde{R}_{zz}(\tau)$ the output autocorrelation. Now using the Fourier Transform of the autocorrelation we obtain the power spectrum, expression (3-3).

$$\tilde{S}_{zz}(\omega) = \int_{-\infty}^{+\infty} \tilde{R}_{zz}(\tau) e^{-j\pi\omega t} \qquad \textit{Eq 3-3}$$

The expressions above shows how easy is to obtain the output power spectrum based on the Gaussian assumption. This also allow a precise and simple analysis of the system behaviour since its possible quantify separately each term and therefore the total

spectrum will be obtained summing each individual term.

3.3 Real Signal Statistics

The Gaussian approximation is acceptable only in the case where several users share the same channel and the resulting signal approaches a normal distribution. However, in CDMA systems this situation is only verified in the direct-link and the assumption of Gaussian behaviour for the reverse-link leads to inaccurate estimates as we saw in previous chapters. So it is important to have an analytical solution with the correct statistic properties of the RF signal. The moments for a QPSK signal were already obtained by Aparin [13]. Here we will present the method to obtain the analytical solution for the M-QAM moments, for any M.

The autocorrelation function of a process *y(t)* is given by:

$$R_{yy}(\tau) = E\left\{y(t)y^*(t+\tau)\right\} = \int_{-\infty}^{\infty} y(t)t(t+\tau)dt \qquad \textit{Eq 3-4}$$

where E[.] is the expectation operator. In this study the I/Q baseband pulse shaped signals are defined as follow:

$$z = \sum_k a_k \, g(t - k \cdot T) \qquad \textit{Eq 3-5}$$

where a_k is a delta dirac function with period T and $L = log2(M)$ different amplitudes with equal probability for a M-QAM system and $g(t)$is the baseband pulse shape filter. The joint moments for two generic processes x and y with the same properties as the one in (3-5), for any (m,n) order is given by:

$$\varphi_{xy}(m,n) = E\left\{x^m(t)y^n(t)\right\} \qquad \textit{Eq 3-6}$$

The bi-dimensional characteristic function of the processes x and y is defined as [9]:

$$M_{xy}(s_1, s_2) = E\left\{e^{s_1 x + s_2 y}\right\} \qquad \textit{Eq 3-7}$$

where s_1 and s_2 are complex variables. Being x and y under the definition used in (3-5) we can rewrite (3-7):

$$M_{xy}(s_1, s_2) = \prod_{k=-\infty}^{+\infty} \prod_{n=-\infty}^{+\infty} E\left\{e^{s_1 a_k g(t-kT)} e^{s_2 a_n h(t-nT)}\right\} \qquad \textit{Eq 3-8}$$

As a_k and a_n have L different amplitudes and $g(t - KT)$ and $h(t - nT)$ are the base band pulse shape filters, the mean value is different from 0 only when $k = n$ and all amplitudes have the same probability, we can solve the expectation operator:

$$M_{xy}(s_1, s_2) = \prod_{k=-\infty}^{+\infty} \left[\frac{1}{M} \sum_{i=1}^{L} \left[e^{a_i [s_1 g(t-kT) + s_2 h(t-kT)]}\right]\right] \qquad \textit{Eq 3-9}$$

As each exponential have symmetrical values, in other words exist $L/2$ different absolute amplitudes, we can use the trigonometric simplification:

$$\cos(x) = \frac{e^{jx} + e^{-jx}}{2} \qquad \textit{Eq 3-10}$$

by rewrite (3-9) we can eliminate half of the summand terms:

$$M_{xy}(s_1, s_2) = \prod_{k=-\infty}^{+\infty} \frac{2}{M} \left[\sum_{i=1}^{L/2} \left[\cos\left(a_i [s_1 g(t-kT) + s_2 h(t-kT)]\right)\right]\right] \qquad \textit{Eq 3-11}$$

A useful tool to obtain the joint moments is the derivate of the log characteristic function:

$$\log\left[M_{xy}(s_1,s_2)\right]=\sum_{k=-\infty}^{+\infty}\log\left[\frac{2}{M}\left[\sum_{i=1}^{L/2}\left[\cos\left(a_i\left[s_1\,g(t-kT)+s_2\,h(t-kT)\right]\right)\right]\right]\right] \qquad \textit{Eq 3-12}$$

which give the *(m,n)* order joint cumulant, $\lambda_{xy}(m,n)$:

$$\lambda_{xy}(m,n)=(-j)^{m+n}\cdot\left.\frac{\partial^{m+n}\ln\left[M_{xy}(s_1,s_2)\right]}{\partial s_1^m\,\partial s_2^n}\right|_{s_1,s_1=0} \qquad \textit{Eq 3-13}$$

This term will be calculated numerically for all requested *(m,n)* order. To relate the joint cumulants with the joint moments we use expression (3-14) from [14]. Like in the cumulants also the odd $m+n$ moments are null, and $\varphi_{xy}(0,0)=1$.

$$\varphi_{xy}(m+1,n)=\sum_{i=0}^{m}\sum_{j=0}^{n}\binom{m}{i}\binom{n}{j}\varphi_{xy}(m-i,n-j)\lambda_{xy}(i+1,j) \qquad \textit{Eq 3-14}$$

We are able to obtain the moments for any order in M-QAM system. So if we have a PA described by a third order polynomial model, we can obtain the linear, correlated and uncorrelated distortion terms as follows, expressions (3-15), (3-16), and (3-17) respectively:

$$R_{y_1y_1}(\tau)=a_1^2\,E\{[i(0)+q(0)][i(\tau)+q(\tau)]\} \qquad \textit{Eq 3-15}$$

$$=2a_1^2\,E\{i(0)i(\tau)\}$$

$$R_{y_1y_{dist}}(\tau)=4a_1a_3\left[E\left\{i(0)i(\tau)^3\right\}+3E\{i(0)i(\tau)\}E\left\{q(\tau)^2\right\}\right] \qquad \textit{Eq 3-16}$$

$$R_{y_{dist}y_{dist}}(\tau) = 2a_3^2 \begin{bmatrix} E\{i^3(0)i^3(\tau)\} + 6E\{i^3(0)i(\tau)\}E\{q^2(0)\} \\ +9E\{i^2(0)i^2(\tau)\}E\{q(0)q(\tau)\} \end{bmatrix} \qquad \textit{Eq 3-17}$$

Where y_1 is the output linear part and y_{dist} the output distorted part. Finally to obtain the spectrum mask the Fourier transform is applied to each term.

Chapter 4

4 EVM estimation

The final objective of the system behaviour prediction is the knowledge of the distortion levels generated and therefore the restrictions that must be imposed to the RF Wireless circuits. The way to quantify the distortion is through figures of merit.

EVM is a very useful figure of merit for systems that use RF digitally modulated signals, since EVM can be directly related with SNR and thus with the distortion introduced by the nonlinear devices. In this Chapter we will quantify directly or indirectly the EVM for the memoryless model, for the Winner-Hammerstein model and for the memory case the multi-slice model, each one representing a distinct effect responsible for the distortion on the PA.

4.1 Relate EVM with IP3

In this section we will quantify the influence of a memoryless nonlinear power amplifier in EVM, other authors [44] had already performed the same analysis but in the frequency domain, here we use a time domain approach which gives a better sensibility on how the different system parameters influence the system response. To describe the memoryless PA behavior we use the mathematical model presented in (4-1) to simplicity we truncate the nonlinear response to the third order, this is enough to get a complete idea of the device influence on the EVM.

$$y(t) = a_1 \cdot x(t) + a_2 \cdot x(t)^2 + a_3 \cdot x(t)^3 \qquad \text{Eq 4-1}$$

Where a_1 is the linear gain, a_2 and a_3 the second and third order nonlinear coefficients,

x(t) is the input RF digitally modulated signal and *y(t)* RF output signal.
The even order terms generate components at baseband and at even order harmonics of the carrier frequency, so a_2 could be rejected since we only pretend in-band components. We will also quantify a1 as being part of the signal therefore.

The memoryless output complex envelope signal is given by:

$$\tilde{y}(t) = (X_i(t) + j \cdot X_q(t)) \cdot \left[a_1 + \frac{3}{4} \cdot a_3 \cdot (X_i^2(t) + X_q^2(t)) \right] \quad \text{Eq 4-2}$$

Where *Xi(t)+jXq(t)* are the complex envelope of *x(t).*
To obtain EVM we sample (4-2), in the optimal instants, leading to the discrete form (4-3):

$$\tilde{y}(k) = \sum_{k=-\infty}^{+\infty} \left[(X_i(k) + j \cdot X_q(k)) \cdot \left[a_1 + \frac{3}{4} \cdot a_3 \cdot (X_i^2(k) + X_q^2(k)) \right] \right] \quad \text{Eq 4-3}$$

This result shows when a digital modulated signal with a constant time domain complex envelope like a QPSK signal is submitted to a memoryless device (which can be modeled by a polynomial response), only a linear deviation in the constellation diagram (a power scale) is introduced. Therefore there is not EVM degradation, by another words all distortion introduced by the nonlinear device are correlated.
Rewriting (4-3) we have:

$$EVM = \sqrt{\frac{\sum_{k=1}^{N} \left[\left(X_i(k) - X_i(k) \cdot cte(k) \right)^2 + \left(X_q(k) - X_q(k) \cdot cte(k) \right)^2 \right]}{\sum_{k=1}^{N} \left[X_i^2(k) + X_q^2(k) \right]}} \quad \text{Eq 4-4}$$

with:

$$Cte(k) = \left[a_1 + \frac{3}{4} \cdot a_3 \cdot (X_i^2(k) + X_q^2(k)) \right] \quad \text{Eq 4-5}$$

Considering that a_1 is part of the desired signal:

$$EVM = \sqrt{\frac{\sum_{k=1}^{N} \left[\left(X_i(k) \cdot (a_1 - cte(k)) \right)^2 + \left(X_q(k) \cdot (a_1 - cte(k)) \right)^2 \right]}{a_1^2 \cdot \sum_{k=1}^{N} \widetilde{P}_{in}(k)}} \quad \text{Eq 4-6}$$

$$= \sum_{k=1}^{N} \frac{3 \cdot a_3}{4 \cdot a_1} \cdot \widetilde{P}_{in}(k)$$

With, $\widetilde{P}_{in}(k) = X_i^2(k) + X_q^2(k)$, and $k = 1,..,N$

Where N is the number of different constellation symbols, and so (4-6) is a sum for each different constellation symbol. As an example, in a QPSK signal we just have to perform one symbol since they all have the same complex envelope power.

For a 16-QAM we have to calculate three symbols, where one of which has the double probability of occur due to the existence of two symbols in the constellation having the same complex envelope power.

We can also establish a relationship with the helpful figure of merit IP3. From [45] we know that IP3 is given by:

$$IP3 = \frac{2}{3} \cdot \frac{a_1^3}{a_3} \quad \text{Eq 4-7}$$

IP3 is a good figure of merit to introduce in the EVM calculations since it describes nonlinearity of a power amplifier as it is a quantify specified by the manufacturer.

So the EVM can be related with IP3 as follow:

$$EVM = \sum_{k=1}^{N} \frac{a_1^2}{2 \cdot IP3} \cdot \widetilde{P}_{in}(k) \quad \text{Eq 4-8}$$

4.2 Impact on EVM of a LTI filter

A Linear Time Invariant, LTI, filter for the in-band frequencies can be simplified by its low-pass equivalent, LPE, transfer function in the frequency domain as:

$$H(w) = |H(\omega)| \cdot e^{-j\left[\theta_0(\omega)+\Delta\theta\right]} \quad \text{Eq 4-9}$$

Where $|H(\omega)|$ is the filter attenuation, $\theta_0(\omega)$ the linear part of the phase which varies linearly with frequency and $\Delta\theta$ the phase offset which introduces a phase shift in the in-band frequencies. The attenuation and the phase shift will increase the EVM, introducing a compression and a rotation in the constellation diagram respectively, and these effects will be independent of the signal form.

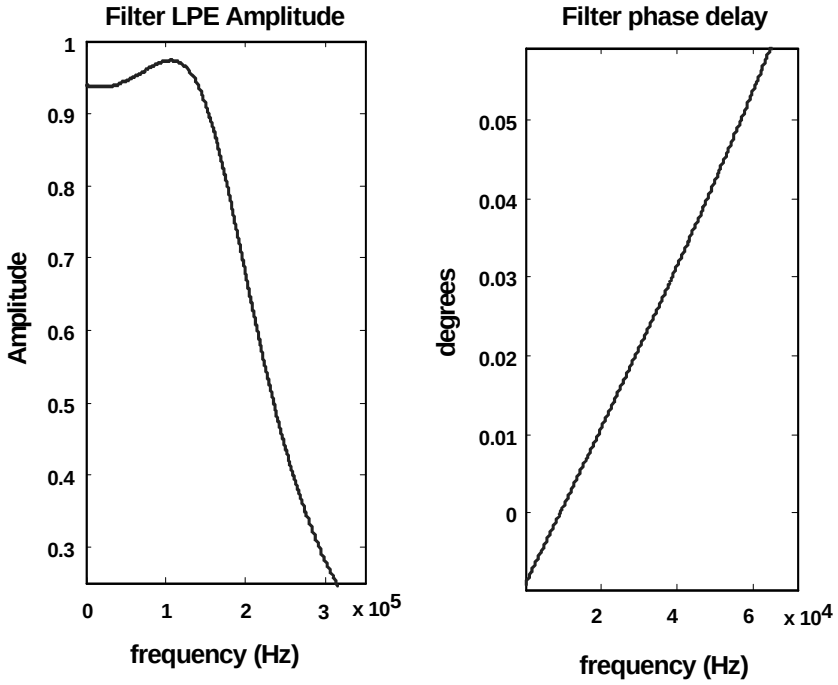

Fig. 8 - Amplitude and phase response of the filter LPE

In order to quantify the effect imposed by the RF filter in the EVM we apply the low-pass equivalent transformation to the filter transfer function, which consists in the translation of the RF spectrum to base band using the follow procedure [46]:

1. Decompose the transfer function $H(\omega)$ using the partial fraction expansion.

2. Discard the poles that are located on the negative-frequency half-plane.

3. Shift the poles located on the positive-frequency half-plane to the zero axis by substituting $z \to z + e^{j\omega_0}$.

Looking to the phase plot in Fig.8 it can be seen that for DC the phase is different from zero by an amount $\Delta\theta$, so taking the phase in DC we obtain the phase shift responsible for the constellation rotation. For the attenuation we perform the in-band amplitude mean value of the filter low-pass equivalent.
In practice, to improve the computation efficiency, we can excite the filter with a test signal and then apply the low-pass equivalent to the input and output signal in order to extract the phase shift and attenuation, as using (4-10) and (4-11) respectively.

$$\Delta\theta = \angle \max(R_{\tilde{x}_{in}\tilde{x}_{out}}(\tau)) \qquad \text{Eq 4-10}$$

$$att = \frac{\mathrm{Re}\left\{\max(R_{\tilde{x}_{out}\tilde{x}_{out}}(\tau))\right\}}{\mathrm{Re}\left\{\max(R_{\tilde{x}_{in}\tilde{x}_{in}}(\tau))\right\}} \qquad \text{Eq 4-11}$$

Where $R_{xy}(\tau)$ is the cross correlation between signal x and y. For precise phase shift estimation we must compensate the attenuation introduced in the output signal.
The test signal can be any signal, as a QPSK modulated waveform, or the usual and easy to use laboratory two-tone test signal. It is important to note that the precision which determines the filter parameters is essential to the correct prediction of the device behaviour.

4.3 Extract EVM for a Winner-Hammerstein Model

The WH model is composed by the cascade: pass band filter, polynomial memoryless nonlinearity, and pass band filter, respectively, Fig. 9. This causes a phase rotation (due to filters phase shift) beyond the known amplitude expansion and compression phenomena.

To quantify the degradation introduced in the EVM by the WH model, we use the expressions shown in (4-6), (4-10) and (4-11), with the parameters for the first filter, $(\Delta\theta_1, att_1)$, the amplifier, (a_1, a_3), and the second filter, $(\Delta\theta_2, att_2)$.

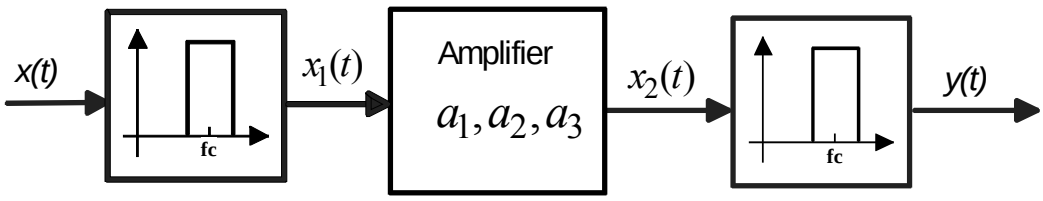

Fig. 9 - Wiener-Hammerstein model

To explain the procedure, a QPSK (4-QAM) signal. However this method can be directly extended to a more complex diagram constellations, as M-QAM with M greater than 4, performing only the sum of the several symbols with different complex envelope powers.

The analysis starts by making *x(t)* pass through the first filter with parameters $(\Delta\theta_1, att_1)$, which leads to the following complex envelope components:

$$\tilde{x}_{q1} = att_1 \cdot \sqrt{X_i^2 + X_q^2} \cdot \sin(\theta - \Delta\theta_1) \qquad \text{Eq 4-12}$$

$$\tilde{x}_{i1} = att_1 \cdot \sqrt{X_i^2 + X_q^2} \cdot \cos(\theta - \Delta\theta_1)$$

The first part refers to a compression due to the filter attenuation and the second to the phase shift, where:

$$\theta = arctg\left(\frac{X_q^2}{X_i^2}\right) \qquad \text{Eq 4-13}$$

With the first RF filter effect quantified, x_1, we are able to apply (4-6), and analyze the memoryless device. So we obtain:

$$\widetilde{x}_2 = (x_{i1} + j \cdot x_{q1}) \cdot \left[a_1 + \frac{3}{4} \cdot a_3 \cdot att_1^2 (X_i^2 + X_q^2) \right] \qquad \text{Eq 4-14}$$

Finally x_2 will pass through the second filter and the output signal $y(t)$ is obtained:

$$\widetilde{y}_q = \left[a_1 + \frac{3}{4} \cdot a_3 \cdot att_1^2 \cdot \widetilde{P}_{in} \right] \cdot att_2 \cdot \sqrt{x_{i1}^2 + x_{q1}^2} \cdot \sin(\theta - \Delta\theta_1 - \Delta\theta_2) \qquad \text{Eq 4-15}$$

$$\widetilde{y}_i = \left[a_1 + \frac{3}{4} \cdot a_3 \cdot att_1^2 \cdot \widetilde{P}_{in} \right] \cdot att_2 \cdot \sqrt{x_{i1}^2 + x_{q1}^2} \cdot \cos(\theta - \Delta\theta_1 - \Delta\theta_2)$$

Now we are able to quantify the degradation introduced by the WH model in the EVM through (4-17), where:

$$\widetilde{P}_{in} = X_i^2 + X_q^2 \qquad \text{Eq 4-16}$$

It's convenient to remember again that (4-17) can be extended for every digital modulation scheme, being only necessary to calculate all different constellation symbols resulting (4-17) under the square root a summation of the different constellation symbols.

$$EVM = \sqrt{\frac{\left[X_i - \left(att_2 \cdot \left[a_1 + \frac{a_1^3}{2 \cdot IP_3} \cdot att_1^2 \cdot \widetilde{P}_{in}\right] \cdot att_1 \cdot \sqrt{\widetilde{P}_{in}}\right)\cos(\phi)\right]^2 + \left[X_q - \left(att_2 \cdot \left[a_1 + \frac{a_1^3}{2 \cdot IP_3} \cdot att_1^2 \cdot \widetilde{P}_{in}\right] \cdot att_1 \cdot \sqrt{\widetilde{P}_{in}}\right)\sin(\phi)\right]^2}{\widetilde{P}_{in}}} \quad \text{Eq 4-17}$$

Where

$$\phi = \theta - \Delta\theta_1 - \Delta\theta_2 \quad \text{Eq 4-18}$$

4.4 Impact of Memory Effects in EVM

With present day demands in wireless systems, the PA must deal with high bandwidths and complex modulation techniques resulting in the introduction of new kinds of effects which leads the behavioural models used until now to lose its accuracy. A usual phenomena seen in today's PA associated to the referred increase in signals bandwidth are the memory effects. These effects can be divided in two types long term and short term, the first has an impact on the signal envelope and the latter of the two has an impact on the RF carrier. In digitally modulated signals the information is carried by the envelope, so it is of primordial importance understand and predict this effect in order to reduce it impact in the overall system performance.

The long term memory effects arise from low frequency behaviour of PA, trapping effects, device thermal response, but the most important contribution for the memory effects is the bias networks, which impose a very low frequency response to the output/input of a nonlinear circuit. This phenomenon is thus nothing more than a feedback mechanism that imposes nonlinear distortion inside the band of interest, by somehow up-convert the low frequency behaviour of the PA to the in-band RF frequency.

A system level model used to represent the long term memory effects was propose by [19], as we said above this model already proved it validity [20] presenting quite good results when applied to a PA presenting memory effects coming from the bias networks. The model is presented in Fig 10, where *x(t)* is the RF digitally modulated signal.

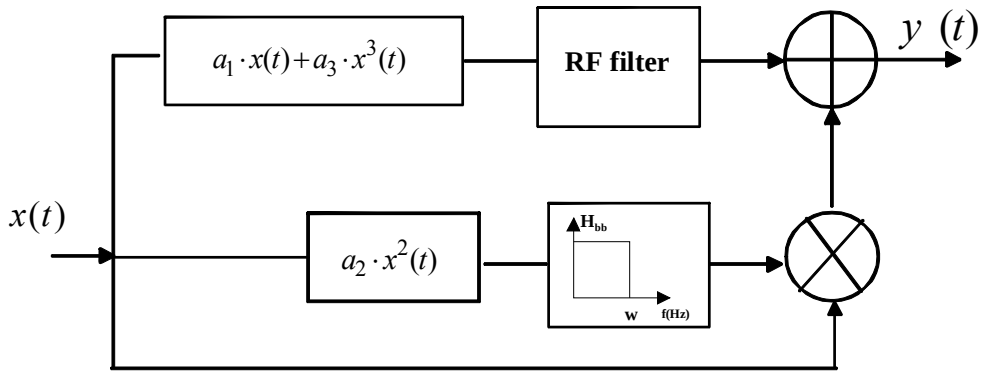

Fig. 10 - Proposed Behavioural model with long term memory effects

This model tells us that the output signal is given by[6]:

$$y(t) = a_1 \cdot x(t) + a_2 \cdot x(t) \cdot \left[\int_{-\infty}^{+\infty} x^2(t-\tau) \cdot h_{bb}(\tau)\, d\tau \right] + a_3 \cdot x^3(t) \qquad \text{Eq 4-19}$$

Which when compared with a memoryless nonlinearity includes the second term that is responsible for the up-conversion of the low frequency behaviour of the PA.

Based on the work presented in [20] it is already known that the fundamental of zone nonlinear distortion can be described by[7]:

$$H_3(\omega_x, \omega_y, -\omega_z) = K - F_2(\omega_x, -\omega_z) - F_2(\omega_y, -\omega_z) \qquad \text{Eq 4-20}$$

[6] In this case we consider that the impact of the RF filter can be ignored.

[7] Similar assumptions as was used in [11], where also considered here, that is the second harmonic filter, and the in-band filter are considered flat all over the interesting bandwidth.

where *H3(.)* is the third order nonlinear operator, responsible for the generation of the nonlinear distortion contribution on the in-band channel.

This means that most of the spectrum shape that will appear at the co-channel and adjacent channel will be tailored by the base band shape filter.

Thus it is expected that this behaviour will affect both the correlated and uncorrelated spectrum at the output.

In [47] it was also proved that the correlated part is only affected by terms equal to:

$$H_3(\omega_x,\omega_y,-\omega_y)=K-F_2(0)-F_2(\omega_x,-\omega_y) \qquad \text{Eq 4-21}$$

where *F2(0)* is the equivalent second order function evaluated at 0Hz, or dc, thus memoryless, since it does not change with frequency, and only the term $F_2(\omega_x,-\omega_y)$ is responsible for the memory behaviour.

While for describing the uncorrelated part all the terms appear, and shape the in-band spectrum.

Thus if we have a PA presenting memory excited by a complex modulated signal its output spectrum characteristics will be deeply impacted by the memory of the PA, and can even change deeply its memoryless behaviour.

In order to analyse the uncorrelated and correlated distortion, and since the CDMA IS-95 excitation has a statistical stochastic behaviour, the analysis of its output should be obtained by a carefully study of its statistical characteristics.

A similar approach used by Bendat [48] will be followed. Different values of cross-correlation functions should be obtained both for the input, output and cross-values. The output autocorrelation will be obtained as:

$$R_{yy}(\tau)=E\left[y(t)y^*(t+\tau)\right]=\int_{-\infty}^{\infty}y(t)t(t+\tau)dt \qquad \text{Eq 4-22}$$

where $R_{yy}(\tau)$ is the output autocorrelation and E[.] is the mean value. It should be noticed that:

$$R_{yy}(\tau) = E\left[y(t)y^*(t+\tau)\right] \qquad \text{Eq 4-23}$$

$$= E\left\{\left[y_1(t) + y_{dist}(t)\right]\left[y_1(t+\tau) + y_{dist}(t+\tau)\right]^*\right\}$$

$$= E\left\{\left[y_1(t)\right]\left[y_1(t+\tau)\right]^*\right\} + E\left\{\left[y_1(t)\right]\left[y_{dist}(t+\tau)\right]^*\right\} +$$
$$E\left\{\left[y_{dist}(t)\right]\left[y_1(t+\tau)\right]^*\right\} + E\left\{\left[y_{dist}(t)\right]\left[y_{dist}(t+\tau)\right]^*\right\}$$

From (5-23) we can see that the first term is the linear response, the second and third terms are the correlated part of the output signal with the input, normally the more important term relating to the gain compression and expansion, and the forth term is the nonlinear distortion correlation, usually called in [11] and [13] spectral regrowth, but unfortunately also has some correlated components with the linear part of the output.

This is in fact one of the major problems of nonlinear systems, that is how to identify the signal component at the output.

One of the solutions often used is to consider as signal the output component which is correlated with the input, as is usual in conventional wireless rake receivers.

Bussgang's Theorem [13, 47, 49] give us the theoretical support for this, since by correlating the output and input signals, we can estimate the effective signal component of the output, and thus by subtraction we can also obtain the uncorrelated part, which is in fact the nonlinear distortion noise.

So for the uncorrelated part exclusively we can also divide the output in:

$$R_{yy}(\tau) = E\left[y(t)y^*(t+\tau)\right] \qquad \text{Eq 4-24}$$

$$= E\left\{\left[y_c(t) + y_u(t)\right]\left[y_c(t+\tau) + y_u(t+\tau)\right]^*\right\}$$

$$= E\left\{\left[y_c(t)\right]\left[y_c(t+\tau)\right]^*\right\} + E\left\{\left[y_c(t)\right]\left[y_u(t+\tau)\right]^*\right\} +$$
$$E\left\{\left[y_u(t)\right]\left[y_c(t+\tau)\right]^*\right\} + E\left\{\left[y_u(t)\right]\left[y_u(t+\tau)\right]^*\right\}$$

$$= E\left\{\left[y_c(t)\right]\left[y_c(t+\tau)\right]^*\right\} + E\left\{\left[y_u(t)\right]\left[y_u(t+\tau)\right]^*\right\}$$

Combining (4-22), (4-23) and (4-24) and using [48] we found that the correlated part of the output could be given by:

$$R_{ycyc}(\tau) = |G_{correlated}|^2 E\left\{[x(t)][x(t+\tau)]^*\right\} \quad \text{Eq 4-25}$$

$$= |G_l + G_{distc}|^2 E\left\{[x(t)][x(t+\tau)]^*\right\}$$

With $G_{correlated}$ what is called the underlying linear system gain, G_l the linear gain and G_{distc} the correlated gain between the output distorted correlated signal and the input signal, which can be further given by:

$$G_{distc} = \frac{E\left\{[y_{dist}(t)][x(t+\tau)]^*\right\}}{E\left\{[x(t)][x(t+\tau)]^*\right\}} \quad \text{Eq 4-26}$$

The uncorrelated part is thus:

$$R_{yuyu}(\tau) = E\left\{[y_{dist}(t)][y_{dist}(t+\tau)]^*\right\} - |G_{distc}|^2 E\left\{[x(t)][x(t+\tau)]^*\right\} \quad \text{Eq 4-27}$$

This is exactly what we are searching when measuring the in-band uncorrelated distortion, and thus the SNDR and ACPR figures of merit.

In the simulated results we have access to each component, so the previous formula can be correctly obtained. Unfortunately in the real world, that is in the measurement counterpart we do not have access directly to the distorted signal, since it is added with the liner output signal, thus the overall underlying linear system gain should be used.

$$G_{correlated} = \frac{E\left\{[y(t)][x(t+\tau)]^*\right\}}{E\left\{[x(t)][x(t+\tau)]^*\right\}} \quad \text{Eq 4-28}$$

In order to clearly understand all phenomena presented, that model was implemented using a path for each nonlinear product, as presented on Fig. 11.

This way each of the nonlinear distortion contribution can be studied individually.
The nonlinear path with constant frequency behaviour (linear and cubic path in Fig. 11), will thus be called memoryless, since they do not change with envelope frequency, and they have been deeply studied by Aparin [13, 50], using a third order polynomial model. In that case the spectrum shape for the correlated and uncorrelated output signal were obtained.
In Fig. 11 the second harmonic filter (not presented), and the in-band filter are considered flat all over the interesting bandwidth, similar assumptions as was used in [20]. So the memory effects are mainly coming from the base-band filtering process up-converted to the fundamental central frequency.

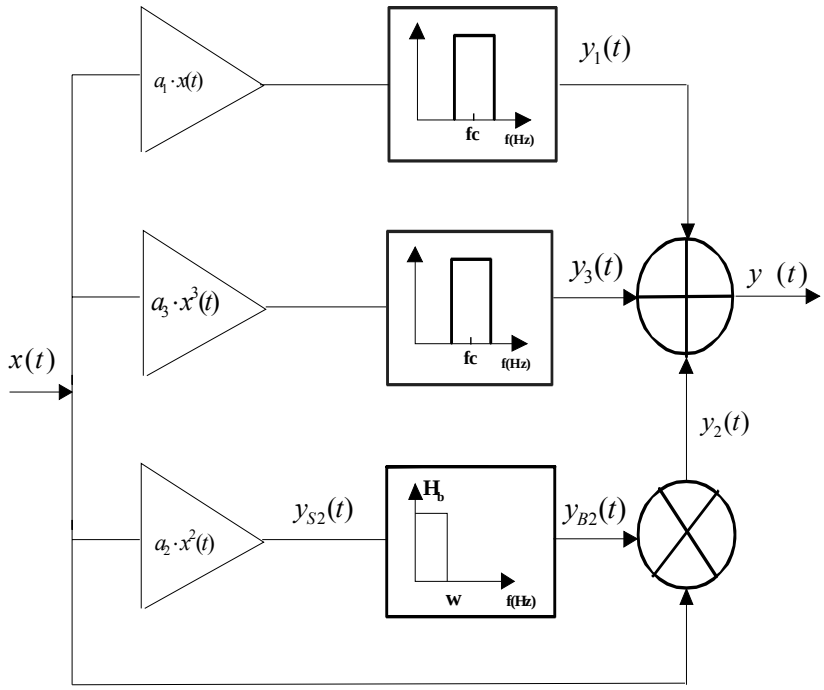

Fig. 11 - Sliced behavioural model presenting memory effects

On the second order path, the signal is first squared (4-29) and filtered out by a base band filter (4-32).

$$y_{S2}(t) = {a_2}/{2}\left(I^2(t)+Q^2(t)+2\,I(t)Q(t)\sin(2w_c t)+\left(I^2(t)-Q^2(t)\right)\cos(2w_c t)\right) \qquad \textit{Eq 4-29}$$

In fact in [50] it is shown that the second order memoryless distortion can be given by:

$$E\left\{I^2(0)I^2(\tau)+Q^2(0)Q^2(\tau)+I^2(0)Q^2(\tau)+I^2(\tau)Q^2(\tau)\right\} \qquad \textit{Eq 4-30}$$

Which as a spectrum of:

$$K|u|\left(1-|u|\right) \qquad \textit{Eq 4-31}$$

where *K* is a constant, and $u=\frac{|\omega|}{2\pi b}$, and b is the bandwidth of the baseband pulse shape filtering.

In our case this signal will now be further filtered by the base band filter. In this case the second harmonic is also filtered out which can not always be true in real PA especially in the wide-band ones.

$$y_{B2}(t)=\frac{a_2}{2}\left[\sum_{k=-\infty}^{\infty}\sum_{n=-\infty}^{\infty} i_k\cdot i_n\cdot \sin c(B\cdot t-n)\cdot \sin c(B\cdot t-k)\right]*\sin c(W\cdot t) \qquad \textit{Eq 4-32}$$

$$+\frac{a_2}{2}\left[\sum_{j=-\infty}^{\infty}\sum_{d=-\infty}^{\infty} q_j\cdot q_d\cdot \sin c(B\cdot t-j+\frac{1}{2})\cdot \sin c(B\cdot t-d+\frac{1}{2})\right]*\sin c(W\cdot t)$$

The base band cut off frequency is W and * represent the convolution operator.

In certain instances, this will destroy the shape of the base band signal. In fact we have used low pass filters, but they can also be high or band pass filters. $y_{B2}(t)$ will then be multiplied by the direct branch $x(t)$ resulting $y_2(t)$ in a modulated carrier around w_c, expression (4-33) present this results.

This time multiplication can also be seen as a spectrum convolution, so the base band filtering process is somehow corrupting the behaviour of the base band shape, and thus will degrade the co-channel distortion.

$$y_2(t)=y_{B2}\cdot\left[\sum_{p=-\infty}^{+\infty} i_p\,\mathrm{sinc}(Bt-p)\cos\left(w_c t+\theta\right)+\sum_{l=-\infty}^{+\infty} q_l\,\mathrm{sinc}(Bt-l+\frac{1}{2})\sin\left(w_c t+\theta\right)\right] \qquad \text{Eq 4-33}$$

Chapter 5

5 Simulation

To show the distortion caused by the phenomena's discussed in the previous chapters some simulations will be performed. First it will be shown that the impact of a nonlinearity in a Gaussian and a QPSK signal is different. This will be shown by simulating a non linear system using ADS, Advanced Design System and Matlab.

5.1 Excitation Signal

In order to have a better understand of the truly impact of a real signal in the degradation of *SNDR* of wireless systems, we use for the simulations and measurements a transmitter based on a real IS-95 reverse-link signal, as presented on Fig. 12. The signal was generated in the ADS and exported to matlab were the different models were developed.

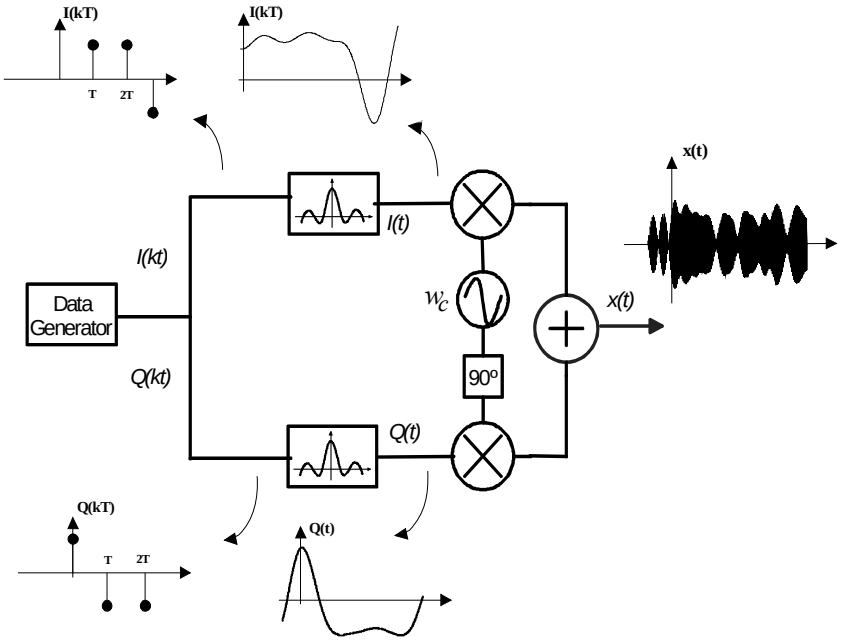

Fig. 12 - I/Q QPSK modulator

The digital information will be in this scenario modelled through a summation of Dirac delta function *δ(t)* with amplitude ±1 and a rate *2B = 1/2T* that is further split into *I* and *Q* channels with rate *B* and filtered out by a raised cosine function *h(t)*,with a cut off frequency of *B/2* as in [13].

For our simple analysis the filter transfer function $h(t)$ can be reasonable represented by a Nyquist ideal pulse-shaping filter, as in (5-1).

$$h(t) = B\frac{\sin(\pi Bt)}{\pi Bt} \qquad \textit{Eq 5-1}$$

Resulting in the follow I and Q components:

$$I(t) = \sum_{k=-\infty}^{+\infty} i_k\, h(Bt-k) \qquad \textit{Eq 5-2}$$

$$Q(t) = \sum_{k=-\infty}^{+\infty} q_k\, h(Bt-k+\frac{1}{2})$$

With i_k and q_k the Dirac delta functions representing the split binary information into *I* and *Q* branches respectively.

The *I/Q* components are further orthogonally modulated by a sinusoidal carrier, the result is depicted in expression (5-3).

$$x(t) = I(t)\cos(w_c t + \theta) + Q(t)\sin(w_c t + \theta) \qquad \textit{Eq 5-3}$$

where ω_c is the angular frequency of the carrier, and θ a random phase.

5.2 Statistic simulations

In the past several authors have addressed the problem of nonlinear distortion in highly complex systems, as a CDMA IS-95 wireless mobile scenario [11], [13], in those previous works several important information have been given to the RF design engineers. First it was found in [13] that the statistics of a that signal is not equivalent to the statistics of narrow band Gaussian noise, Fig.13, which was the usual type of excitation signal used for identifying and extracting behavioural models with nonlinear distortion capabilities.

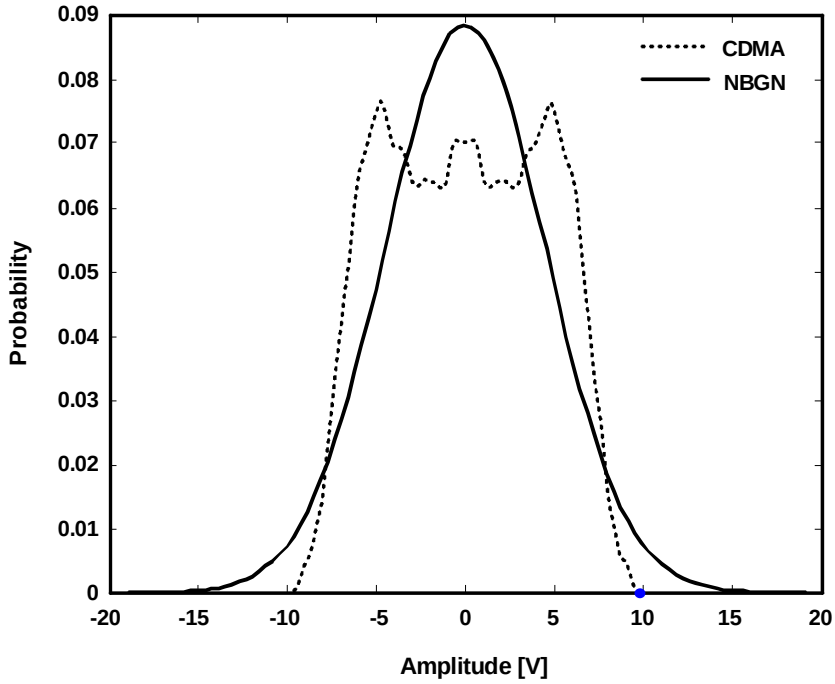

Fig. 13 - Probability Density Function, pdf, of a CDMA and NBGN

In Fig. 14 its clear the difference between a Gaussian process and an IS-95 CDMA signal when both signals pass through a memoryless nonlinearity. The in-band distortion of an IS-95 CDMA signal in a memoryless system, is reduced when compared with the NBGN behaviour, Fig. 14. Moreover the bell shape of the out-of-band distortion usually seen in NBGN is altered, and can even tend to a plateau. This proves the necessity of use a correct statistic to obtain accurate estimates of the systems behaviour.

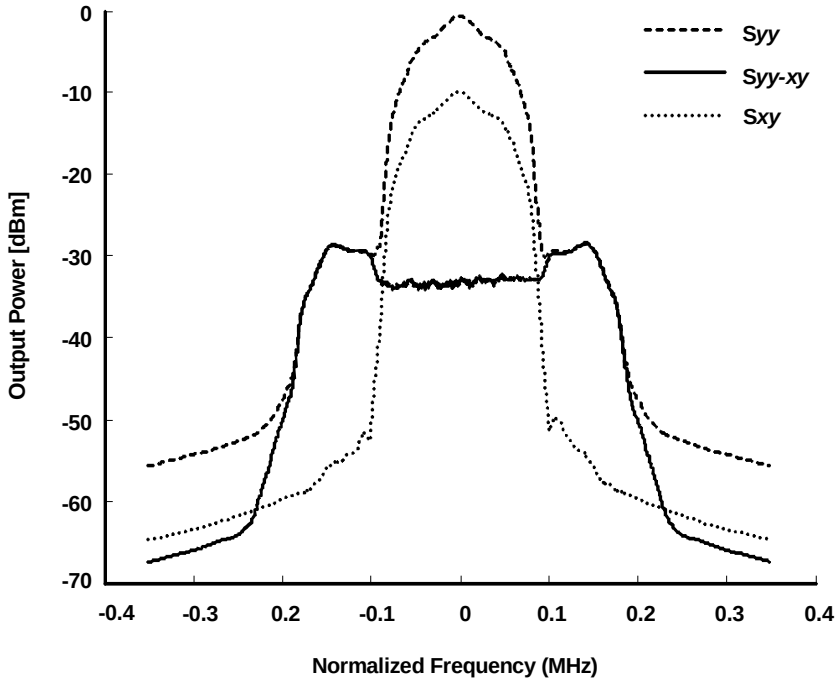

(a)

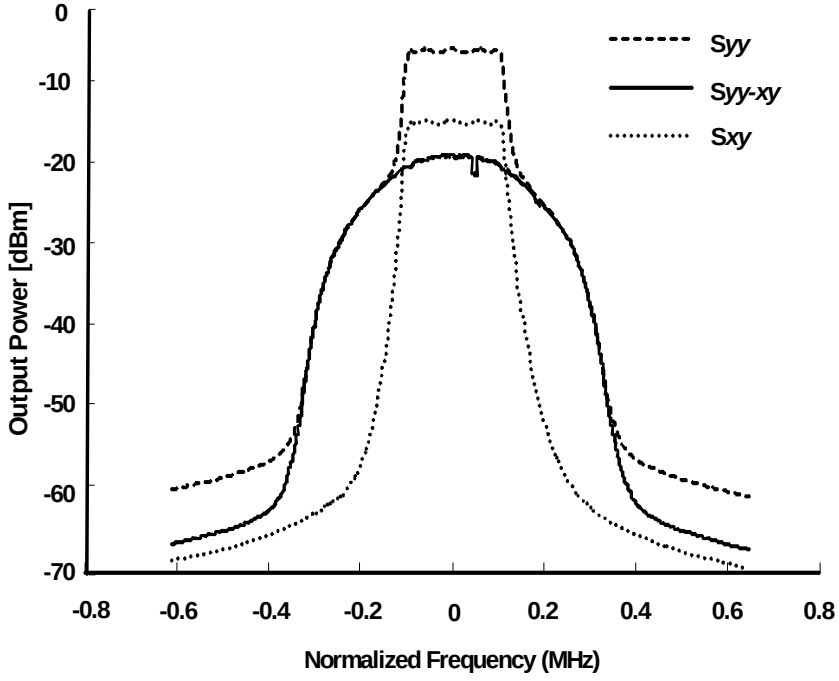

(b)

Fig. 14 - CDMA (a) and NBGN (b) passing through a memoryless nonlinear device

5.3 Memoryless spectrum shape

The results here presented are the well known spectrum shapes of modulated wireless RF signal for weakly memoryless nonlinearities. The results were simulated in ADS using a third order nonlinearity described by a power series as:

$$y(t) = \sum_{n=1}^{N} a_n x^n(t) \qquad \textit{Eq 5-4}$$

Where a_n represents the nth order nonlinearity gain, N is the maximum order of interest, and $x(t)$ the IS-95 reverse-link input RF signal.

For a circuit weakly nonlinearity, the third order term is dominant and higher order terms can be eliminated. Also, even order terms can be eliminated since they do not generate terms around the carrier. However under strong signal conditions this analysis start losing accuracy.

An IS-95 reverse-link signal $x(t)$ was used as the excitation. Fig. 15 presents the input spectrum $X(w)$ around the carrier.

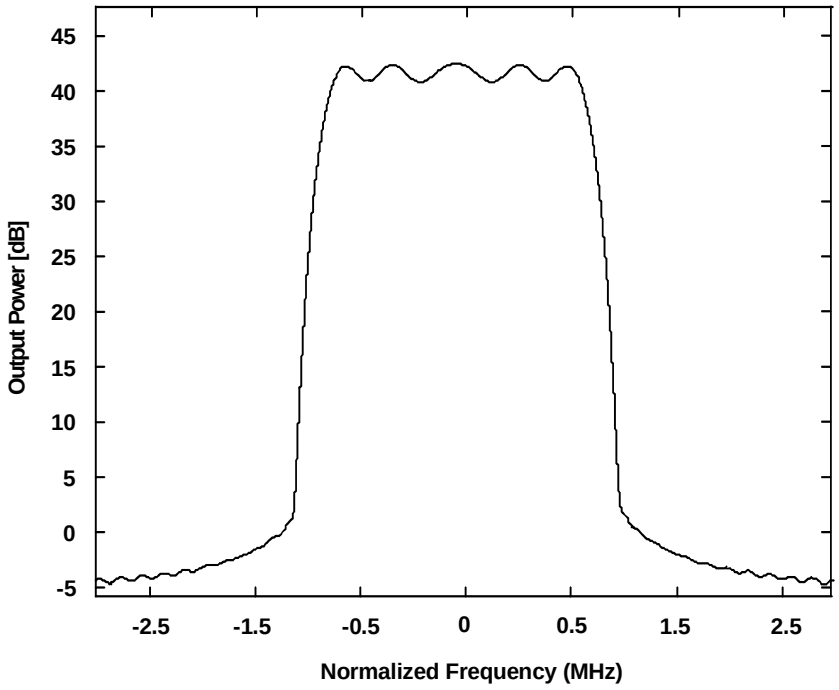

Fig. 15 - Input spectrum of an amplifier for an IS-95 reverse-link signal

Fig. 16 presents the total output spectrum, where the spectrum widening due to the nonlinear terms is visible.

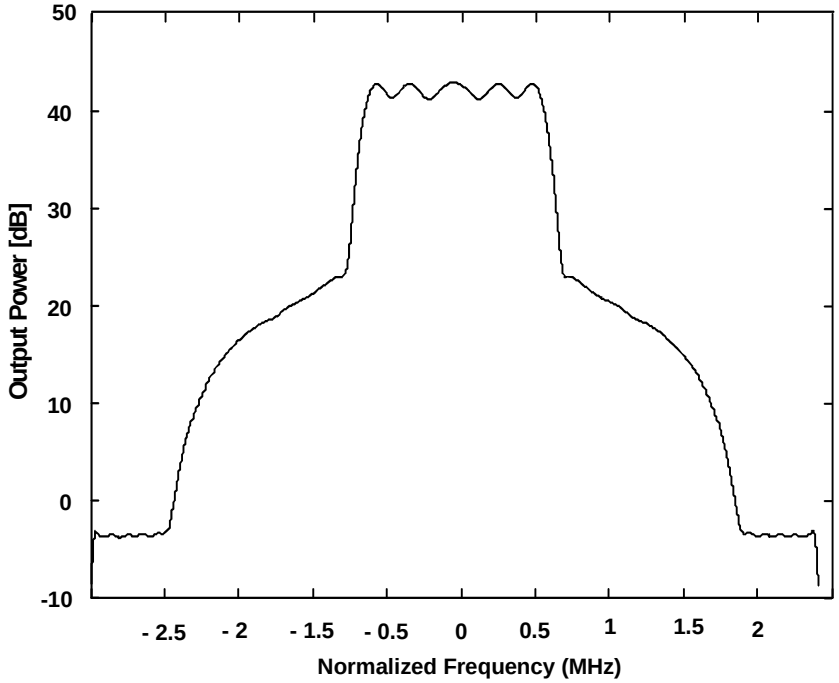

Fig. 16 - Output spectrum of an amplifier for an IS-95 reverse-link signal

Fig. 17 presents the characteristic uncorrelated spectrum shape responsible by the distortion for a third order nonlinearity. The co-channel distortion presents a very characteristic mask, although these format only appears for the reverse link, where we have only one user, as we increase the number of users in the same channel the uncorrelated spectrum tends to a Gaussian shape as we showed above.

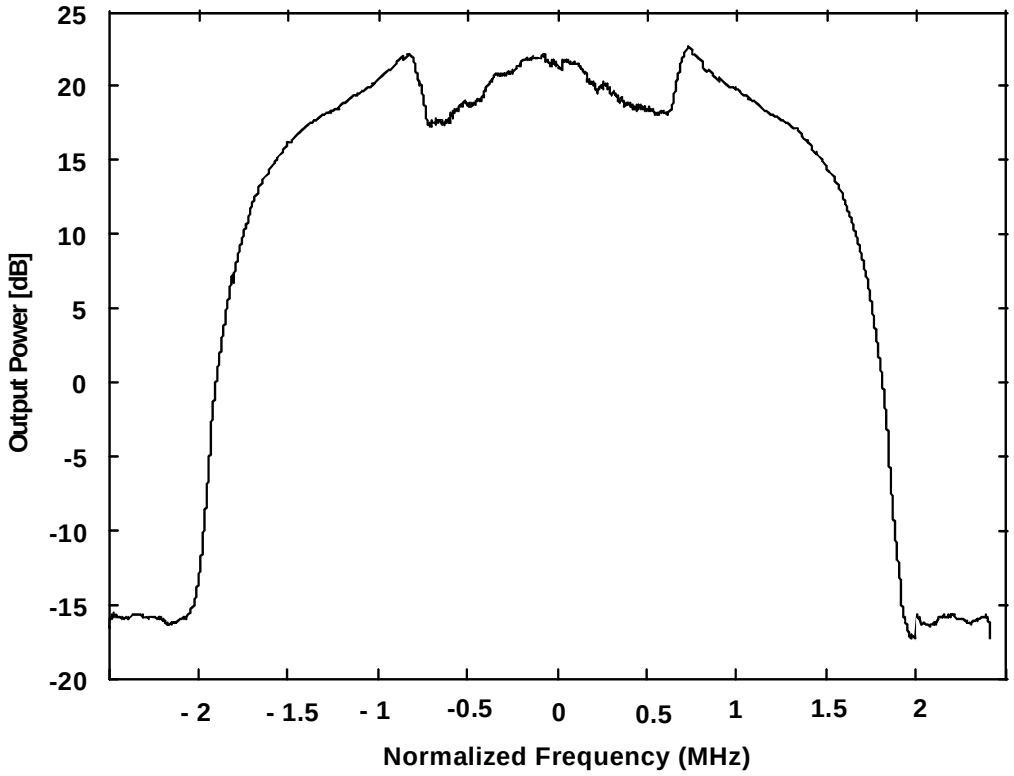

Fig. 17 - Uncorrelated Output spectrum of an amplifier for an IS-95 reverse-link signal

5.4 Winner-Hammerstein simulations

In order to validate the performance of the approximations proposed above, we use SIMULINK [52] and design a 16-QAM transmitter based on the transmitter presented on Fig. 12. The RF filters have two times the signal bandwidth, and the amplifier is described by a third order non linear polynomial model, presenting gain compression. To perform EVM we get the complex envelope (I/Q sequence) of the RF output and input signal at the PA, and applying in (4-17).

The filters' parameters are obtained using the procedure explained above, with two signals captured with probes, one at the input and the other at the output of the filters.

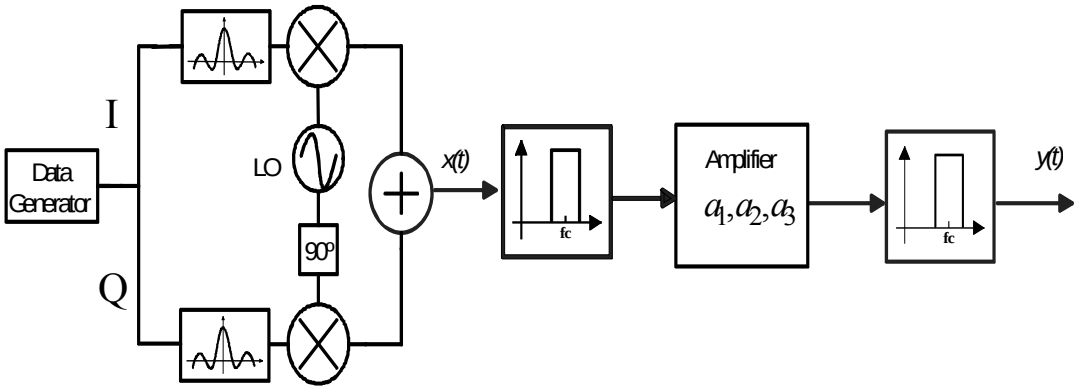

Fig. 18 - QPSK transmitter architecture

Fig. 20 validates the proposed approximation by confirming an excellent approximation between the simulated EVM values and (4-17), we also include the PA AM/AM curve, to give an idea of the PA operating point, Fig. 19.

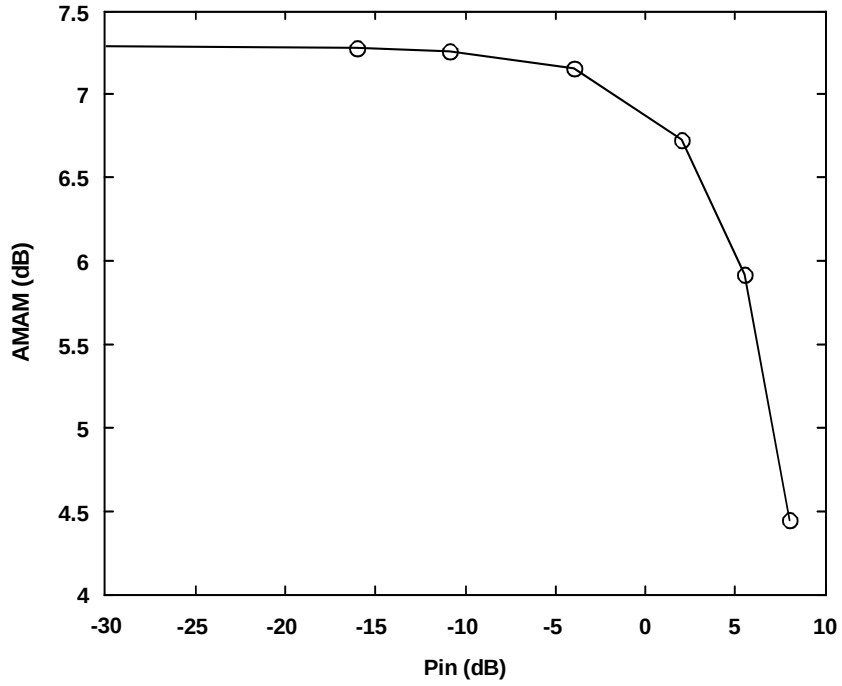

Fig. 19 - System metrics. o : AM/AM

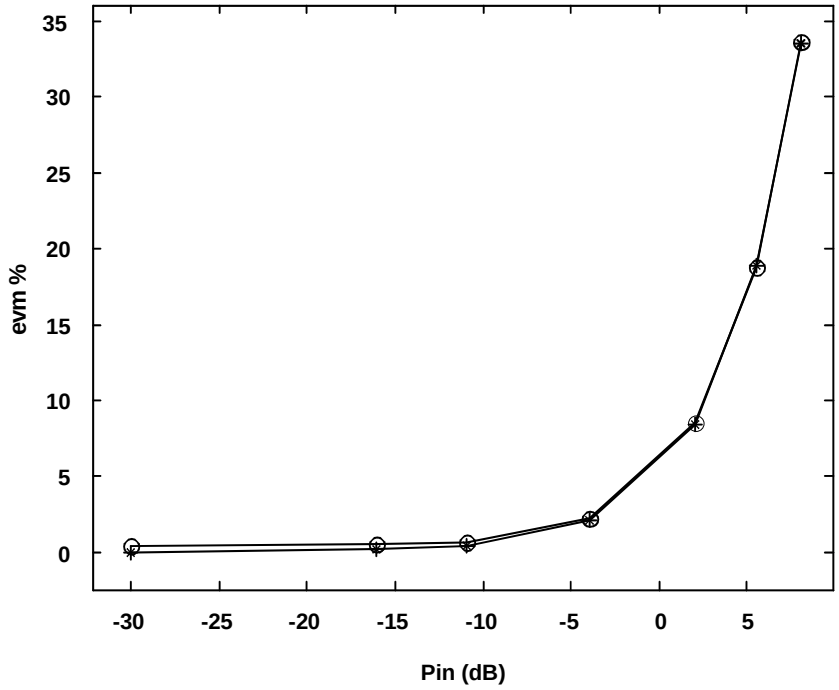

Fig. 20 - 16-QAM, EVM approximation; o : simulated; and * : estimated

5.5 Memory simulations

To simulate the memory effects the scheme presented in Fig. 11 was implemented on ADS. The excitation signal used was the IS-95 reverse-link signal available on the ADS RF System library facility.

On the second order path, the signal is first squared (4-29) and filtered out by a base band filter (4-32), the resultant spectrum of these operations can be seen in Fig. 21 and Fig. 22 respectively.

The shape of the second order distortion can thus be seen in Fig. 21, where it shows a low power valley in the centre frequency, around dc. The dc component comes form square operation which imposes a mean value different from 0.

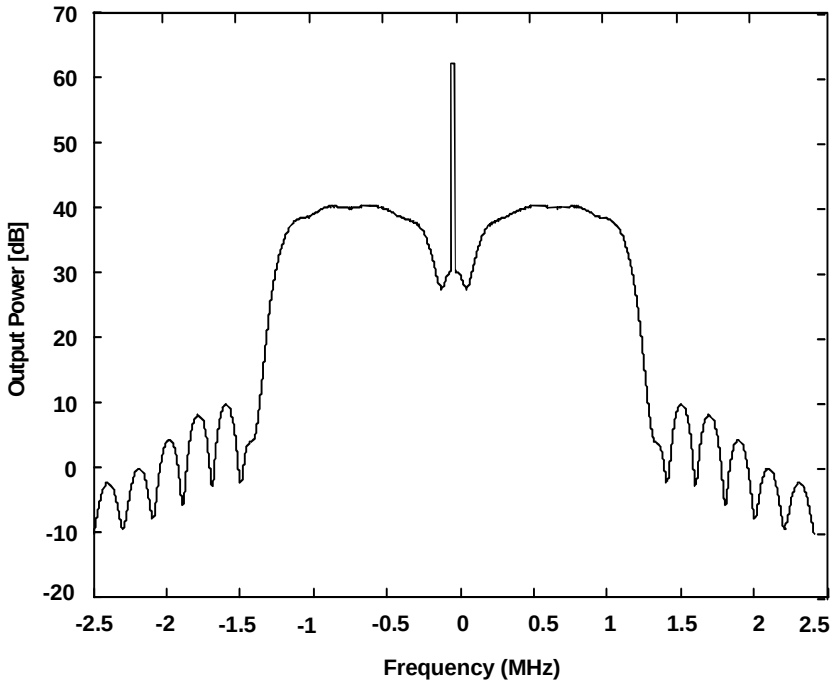

Fig. 21 - Baseband component of the input RF squared signal

The memory effects are introduced by the baseband filter process which can be seen on Fig. 22 for different bandwidths, and in certain instances, this will destroy the shape of the base band signal. In fact we have used low pass filters, but they can also be high or band pass filters.

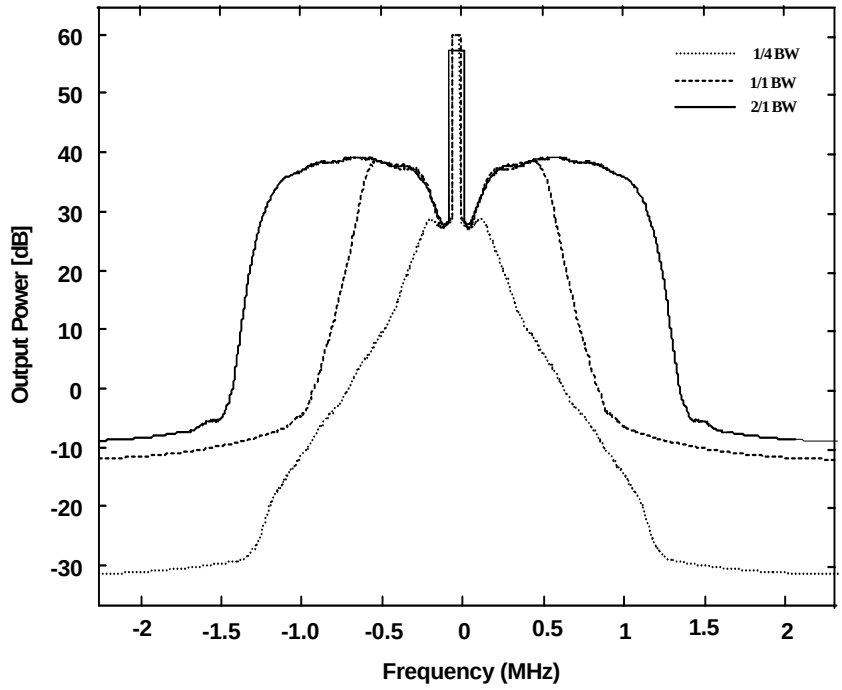

Fig. 22 - Base band component of the filtered input RF squared signal.[8]

The memory effects will press a new spectrum mask both on the co-channel and the spectral regrowth.

Fig. 23 presents the total correlated and uncorrelated spectrum shape for the memory slice.

A strong and perfectly equal (correlated) fundamental RF waveform will appear at the output of the second order path, since this component is derived by the convolution with a dc dirac it does not change with base band frequency. This can be attributed to the fact that this second order path, arises from the convolution of the base band signal with a copy of the RF input waveform.

Regarding the uncorrelated distortion, the different shapes can be attributed to two different causes, as was seen above, first the dramatic change of second order base band spectrum shape due to the base band filtering which not only changes the spectrum, but also the statistic behaviour of the pure second order base band time domain signal.

[8] All simulations were performed for three different base band filters bandwidth, i.e. 1/4, 1/1 and 2/1 of the signal bandwidth.

The case where the filter has ¼ of the signal bandwidth the distortion is reduced since this result from a convolution between the RF input signal and an approximation of a delta Dirac function, due to the narrow base band filter. The larger filter have a form very similar to the memoryless case as we except, the absence of the co-channel bell shape form is due to the no ideal filter behaviour.

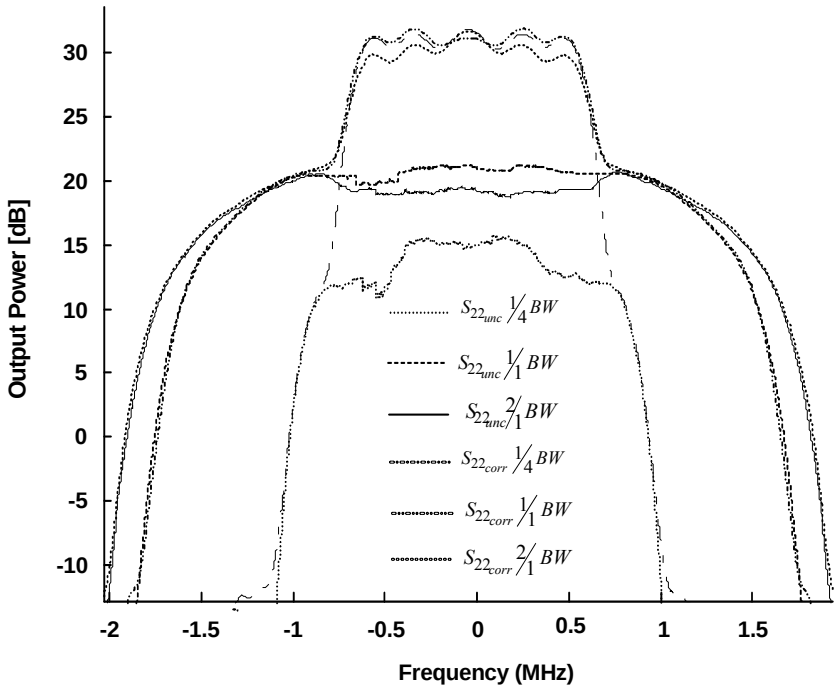

Fig. 23 - Total correlated and uncorrelated spectrum mask arising from the second order memory path

The total output spectrum mask, including the correlated and uncorrelated part, is presented on Fig. 24 for the three different filters, and for the memoryless case.

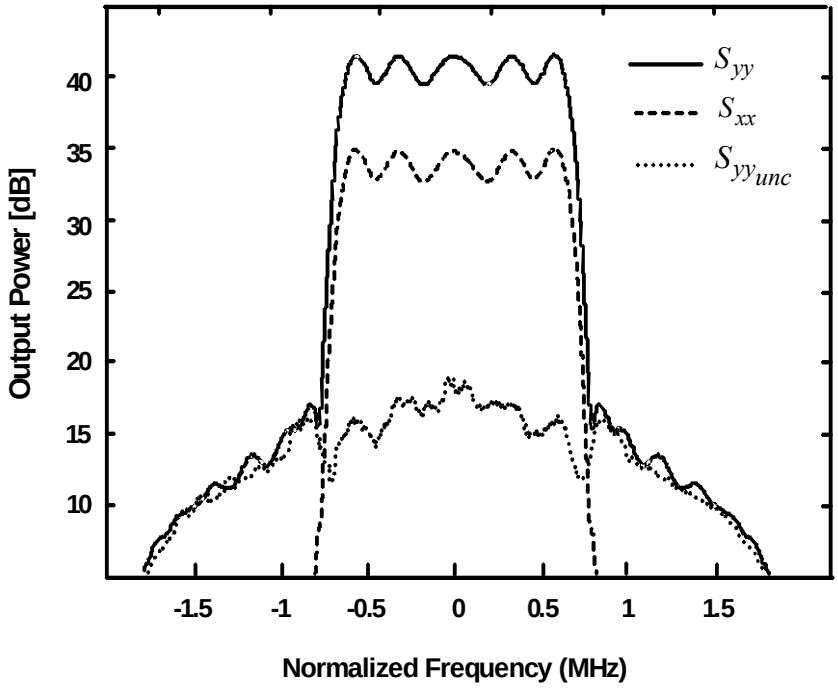
S_{yy}
S_{xx}
$S_{yy_{unc}}$
Output Power [dB]
40
35
30
25
20
15
10
-1.5
-1
-0.5
0
0.5
1
1.5
Normalized Frequency (MHz)

a)

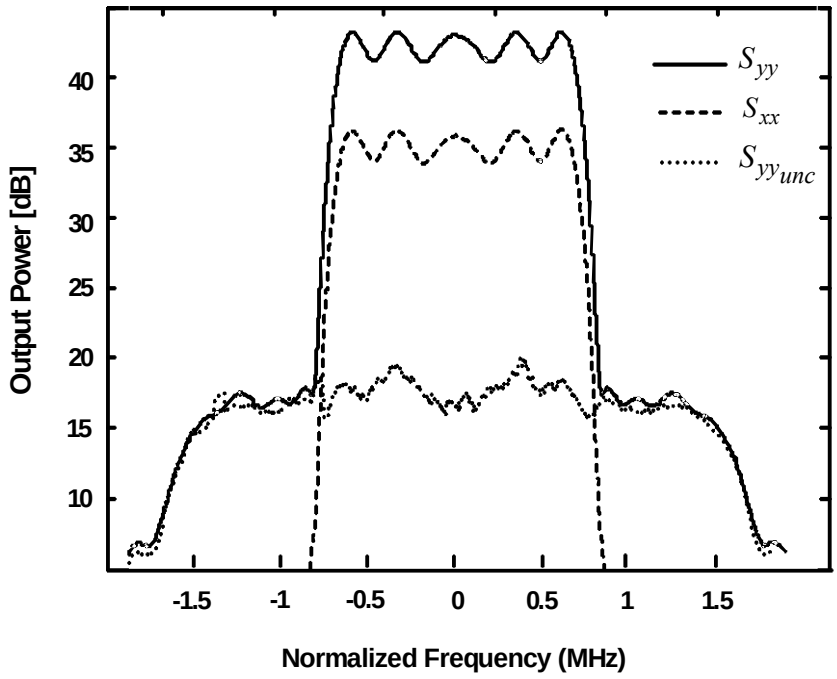
S_{yy}
S_{xx}
$S_{yy_{unc}}$
Output Power [dB]
40
35
30
25
20
15
10
-1.5
-1
-0.5
0
0.5
1
1.5
Normalized Frequency (MHz)

b)

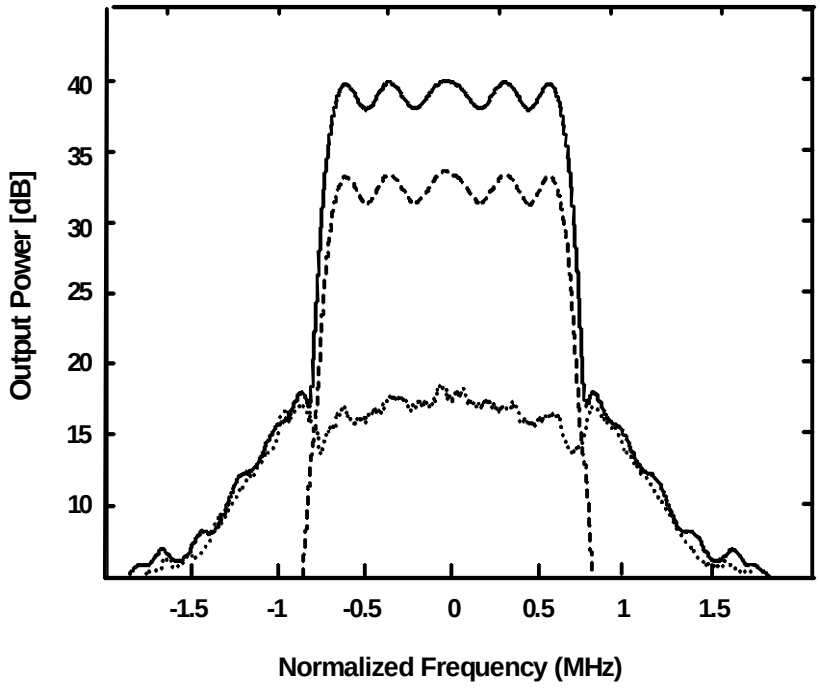

c)

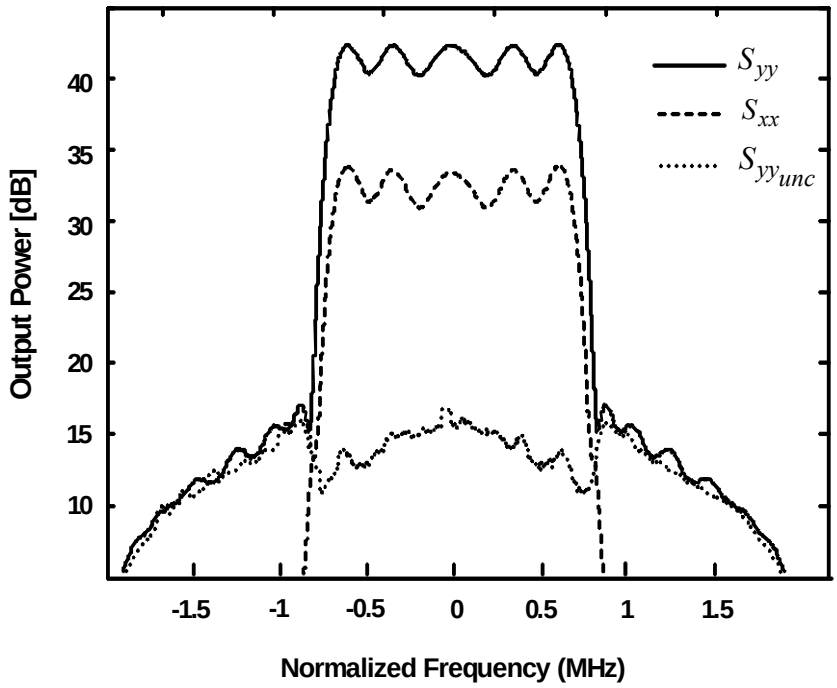

d)

Fig. 24 - Total uncorrelated memory spectrum mask: a)3ª Filter b) 2ª Filter c)1ª Filter d) memoryless

From Fig. 24, it is clearly seen that the distortion in the entire three situations raise compared with the memoryless case.

Moreover it is also seen that both the very narrow band filter and the very wide band filter, have a similar response, since both of them are imposing a low value of uncorrelated distortion arising from the base band path. Actually the narrow band filter is allowing mainly de dc dirac to pass. The large band filter is similar to a memoryless case, where all the base band response is considered, similar as if we have $x(t)^2 x(t) = x(t)^3$.

The mid-band filter is in fact the one that imposes a strong impact on the nonlinear output distortion, since as can be seen, not only the co-channel uncorrelated distortion has change its shape, but also the spectral regrowth as raised significantly compared with the other cases. These is due to the fact that we will make the convolution between the input signal with a very distorted baseband version.

The memory part effect coming from the second harmonic down converted to the carrier frequency can be rejected when compared with the base-band effect up-converted to the carrier frequency. On the other hand the correlated component is equal in the three cases, since all of them arises from the dc dirac convolution.

In order to be able to prove this sentence, the second path, correspondingly to the base band filtered component was tested, when the ½ bandwidth low pass filter was used, in two conditions, one similar to the already presented, and another one where a very narrow band high pass filter is cascaded with the low pass filter, removing this way the dc dirac from the up conversion.

Fig. 25 presents the results for the correlated and uncorrelated distortion of this branch exclusively, before and after the high pass band filter insertion. As can be seen from the Fig. 25 the main contribution for the correlated distortion are coming from the dc dirac that appears at the base band signal due to the ciclo-periodic nature of the QPSK signal. Despite this still exists some residual correlated distortion as can be seen in Fig. 25.

Regarding the uncorrelated distortion different shapes, it can be attributed to two different causes, as was seen above, first the dramatic change of second order base band spectrum shape due to the base band filtering which not only changes the spectrum, but also the statistic behaviour of the pure second order base band time domain signal. Secondly the elimination of the second harmonic of that same path has also a strong

effect on the overall up-conversion.

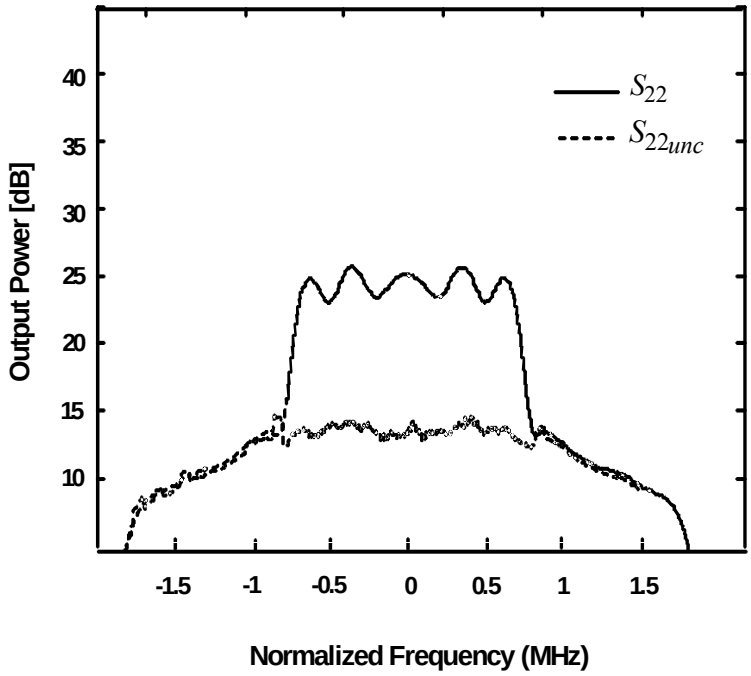

a)

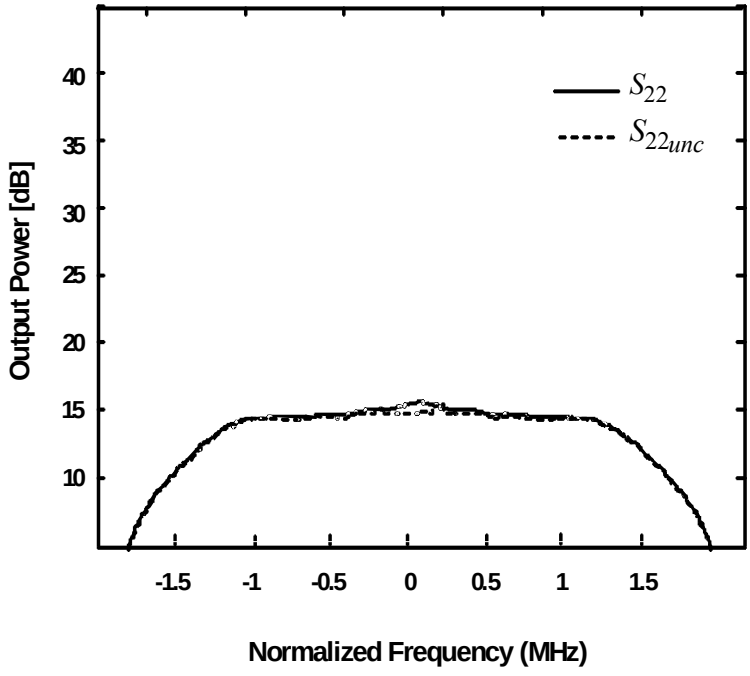

b)

Fig. 25 - Base band path distortion, after the base band filtering a) with low pass filter, b) with high pass followed by low pass filtering.

Chapter 6

6 Measurements

In this chapter some measurements were done to observe the real behavior of the PA. First the procedure used to measure the output RF signal is explained and also the method to split the correlated part of the uncorrelated part. The measurements were done to show the effect of the long term memory effects in CDMA signals.

6.1 Co-channel Distortion Measurement Bench

In order to measure the uncorrelated co-channel distortion, the procedure proposed by Bendat could be followed, and the uncorrelated distortion obtained by using:

$$R_{yuyu}(\tau) = E\left\{[y(t)][y(t+\tau)]^*\right\} - |G_{correlated}|^2 E\left\{[x(t)][x(t+\tau)]^*\right\} \qquad \textit{Eq 6-1}$$

which is an extreme complex analysis if made in the time domain, so the usual way to do it is by first calculate the spectrum of the output and input signal, and the underlying linear system gain in the frequency domain. Thus the output uncorrelated spectrum will be:

$$S_{yuyu}(\omega) = S_{yy}(\omega) - |G_{correlated}(\omega)|^2 S_{xx}(\omega) \qquad \textit{Eq 6-2}$$

This way the output uncorrelated spectra is directly obtained.
The data, input and output signals, are gathered by a Vector Signal Analyser, VSA [53], and then processed in a computer based numerical machine.

Nevertheless this formulation depends on a cancellation between the output signal spectra and the output equivalent linear contribution spectra, however suffering for every numerical error arising from the cancellation procedure.

Actually the calculation of the cross-correlation terms is very intensive, and suffers from a high degree of measurement noise, since several slices of the time domain modulated signal should be acquired before the calculations are done.

Moreover the number of random windows to use is extremely high for a correct identification of the nonlinear co-channel distortion, this is the reason why most of the authors that have dealt with this problem have selected an alternative measurement scheme.

That alternative solution implements the cancellation of the correlated part in the instrumentation itself, rather than in a numerical computer.

One of those instrumentation proposals is based on the application of a feed-forward cancellation loop as presented in [54] and [55], Fig. 26.

The output of this loop is nothing more that the overall output signal (including the distortion), after the reduction of a linear copy of the input signal. The second path of the loop is nothing more than an approximation of the underlying linear gain of the amplifier.

In a memoryless case this path could correctly approximate the linear gain of the system, which is normally approached, by an attenuator followed by a phase shifter (at least for narrow band systems) as was presented in [13, 54-55]. Unfortunately in the case of PA presenting a large impact of memory effects, that is not correct, since the underlying linear system is quite different from a linear well behaved gain [49], and so by applying this feed-forward scheme the output will have a certain amount of correlated distortion that could not be modelled by the delay plus attenuator approach.

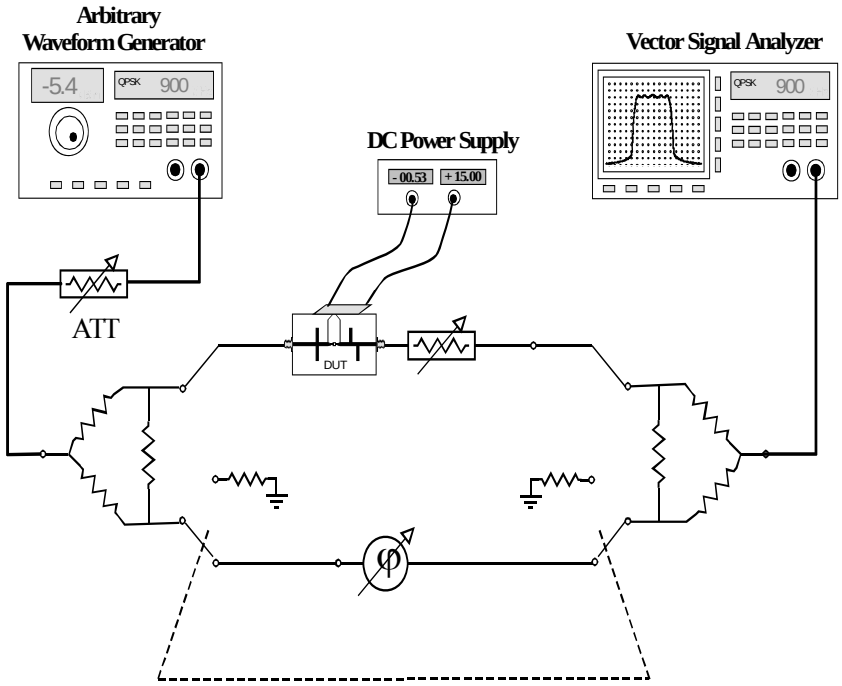

Fig. 26 - Feed forward cancellation technique

Nevertheless after the cancellation we managed to have a strong reduction of the linear signal that most of the times is several dB's above the uncorrelated distortion, so the relationship between correlated and uncorrelated distortion in this case is much smaller, and thus the application of the previous formula is improved in respect to numerical noise.

Consider expression (6-2), if we apply it to the output signal of the cancellation loop as in Fig. 26 the numerical noise will be reduced. Consider the output spectrum power of the signal arising from the cancellation loop:

$$S_{yyloop}(\omega) = S_{yy}(\omega) - \left|G_{memorylesscorr}(\omega)\right|^2 S_{xx}(\omega) \qquad \textit{Eq 6-3}$$

where $G_{memorylesscorr}(w)$ is a linear underlying linear system that includes the pure linear gain and the correlated gain arising from the memoryless nonlinear distortion part.

Looking at expression (4-25) the correlated gain will then be divided into a pure linear part, a correlated linear gain coming out from the memoryless distortion and a component of the correlated memory distortion, as in expression (6-4).

$$\left|G_{correlated}\right|^2 = \left|G_1 + G_{distc}\right|^2 = \left|G_{memorylesscorr} + G_{memorycorr}\right|^2 \qquad \textit{Eq 6-4}$$

which will be all added since they are all correlated.

So in this case, part of the underlying linear gain, was already subtracted from the output and thus the uncorrelated distortion will then be:

$$S_{yuyu}(\omega) = S_{yyloop}(\omega) - \left|G_{memorycorr}(\omega)\right|^2 S_{xx}(\omega) \qquad \textit{Eq 6-5}$$

Since the main part of the underlying linear system comes from the pure linear gain, the amount of correlated signal at the output is now much more reduced, and thus the numerical error will be further diminished, as already stated for the computational case, where uncorrelated distortion is normally calculated directly over the distortion components.

The value of $\left|G_{memorycorr}(\omega)\right|^2$ can then be directly calculated from:

$$G_{memorycorr} = \frac{E\left\{\left[y_{loop}(t)\right]\left[x(t+\tau)\right]^*\right\}}{E\left\{\left[x(t)\right]\left[x(t+\tau)\right]^*\right\}} \qquad \textit{Eq 6-6}$$

and in the frequency domain as:

$$G_{memorycorr} = \frac{S_{yloopx}(\omega)}{S_{xx}(\omega)} \qquad \textit{Eq 6-7}$$

where $S_{yloopx}(w)$ is the cross correlation of the output of the loop and the input signal.

This will thus be the measurement procedure followed in the experimental validation of the work.

6.2 Exprimental Results

In order to see the experimental impact of the memory effects in a QPSK like modulated signal, we have generated an IS-95 CDMA reverse link as the excitation signal and apply it to a PA presenting memory. The set-up is presented in Fig. 26

In order to obtain the memory behaviour and maximize their effects a PA was biased near its large signal sweet spot [56].

The first results are presented in Fig. 27, where the PA behaviour for an input power sweep, both the co-channel and adjacent channel distortions can be seen as well as the SNR.

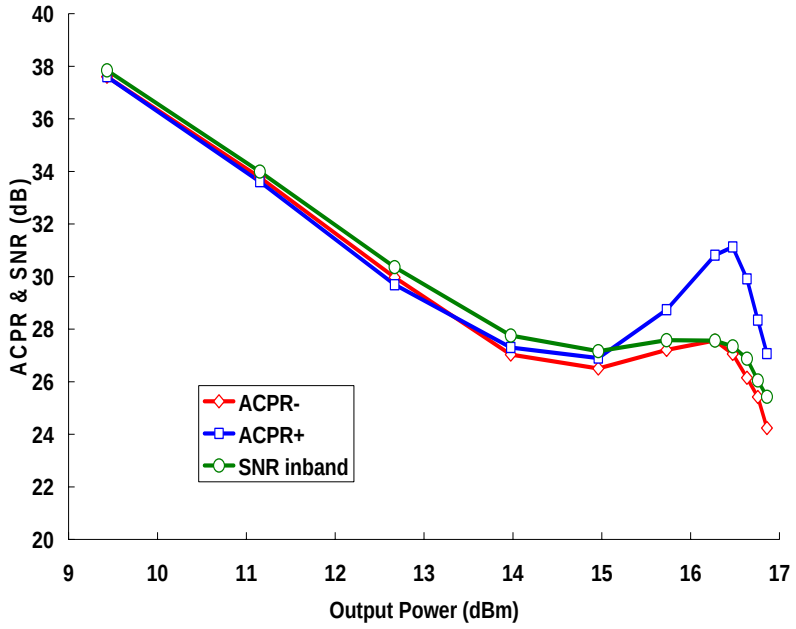

Fig. 27 - IS-95 excitation passed through a PA nonlinearity presenting memory

From the figure it is possible to see a high value of asymmetry, and thus of memory effects in the ACPR values, and by a comparison with the Gaussian behaviour, we see that that it states the viability of the large signal IMD sweet spot use for this respect. An interesting observation that can also be obtained in this graph is that the SNDR also presents a large signal sweet spot, despite it follows the worst behaviour of the ACPR values as expected. Therefore the uncorrelated co-channel distortion is impacted very

similarly as the ACPR.

These result states that the large signal SNDR sweet spot is also visible on IS-95 Systems, even in PA's presenting memory effects.

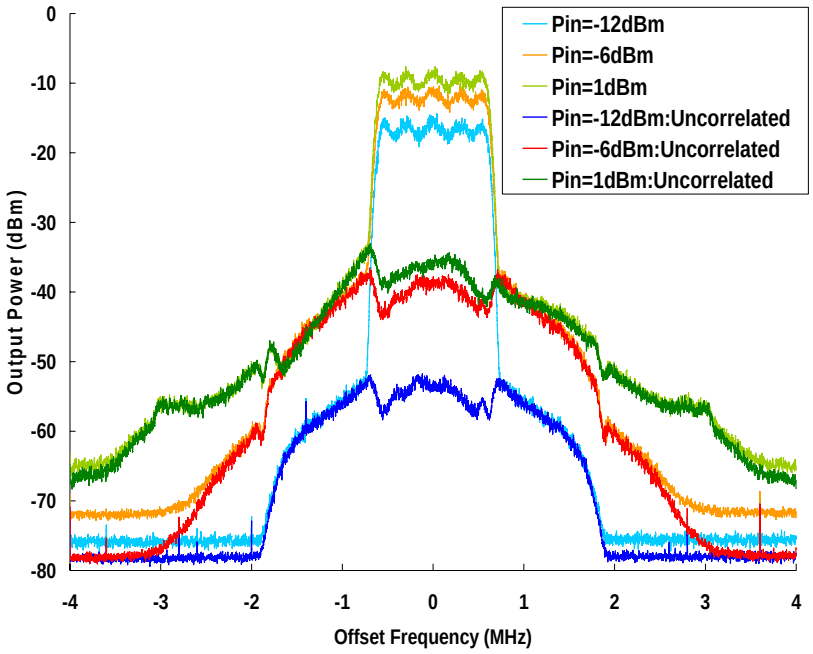

Fig. 28 - Output spectrum of the IS-95 excitation passed through a PA nonlinearity presenting memory

From Fig. 28 complements Fig. 27 where the co-channel distortion is completely different at small signal where no impact of memory effects is visible both at the co-channel and adjacent channel, and at large signal, where a clear impact of memory effects is visible at the adjacent channel asymmetry.

Fig. 29 and 30, presents the seek results, for the case of the PA presenting memory and for a memoryless PA.

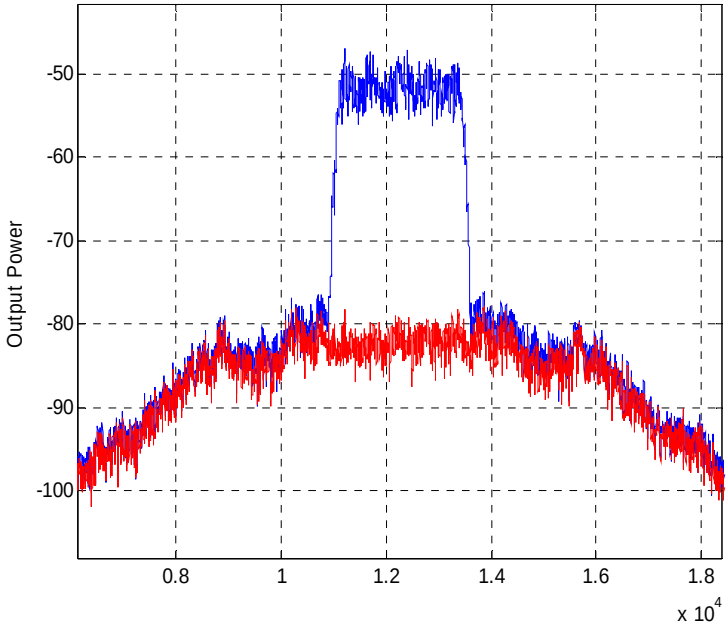

Fig. 29 - IS-95 excitation passed through a PA nonlinearity presenting memory

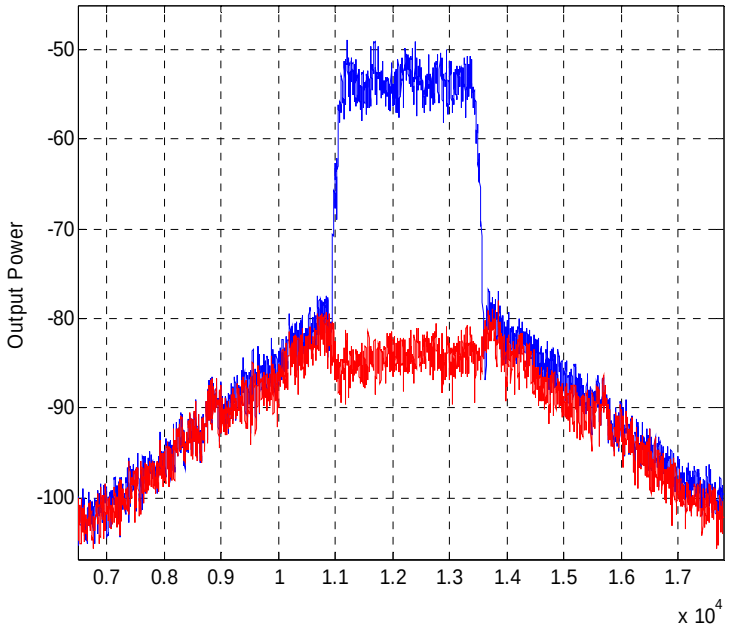

Fig. 30 - IS-95 excitation passed through a memoryless PA nonlinearity

As was expected the memory effect case presents a clear rise both in the co-channel and adjacent channel distortion, degrading in that respect the SNDR.

Chapter 7

7 Conclusions

In this dissertation the statistic nature of the RF signals as well as the degradation of the systems performance when the PA presents several nonlinear phenomena was discussed.

It was proved that a large difference between a Gaussian process and the real statistic signal exists either at the co-channel as also at the adjacent channels. These results have an increased importance since previous works were obtained using the Gaussian assumption to model signals.

We also showed that the study of long term memory effects presents very important differences for both types of signals.

These dissertation also studied the effects of several phenomena presented in PA´s, first the analysis of the memoryless model was made described by a third order polynomial model, after, a more realistic model was analysed introducing constellation rotations, the Winner-Hammerstein model, reducing the E_b/N_o relationship. Finally the long term memory effects associated to the bandwidth increase on the nowadays wireless systems was deeply studied.

We observed that the memory effects have a strong impact in the wireless systems. It can compromise the system performance as we saw trough the rise of the distortion levels. We also show that the asymmetries due to the long term memory effects appear in strong signal conditions, this effect appears both in the co-channel as in the adjacent channel components. We also confirm the existence of sweet spot for a PA when present long term memory effects and in real signal excitations.

7.1 Future Work

To complete the study presented in this dissertation and completely characterize the wireless systems at System level point of view, involving digital modulated signals passing through nonlinear devices, is necessary to obtain the statistic of M-QAM signal for any indice M, which will allow an accurate analysis of the following subjects.

First a deep study in order to quantify and understand the PAPR for a CDMA system must be done since all analyzes made uses the Gaussian assumption, as we saw, this assumption leads to a very distinct results in relation to the real statistics.

Secondly the study done by Aparin for the memoryless model using the real moments for a CDMA system should be extended to the memory model

References

[1] Peyton Z. Peebles, Digital Communication Systems, Prentice Hall, 1987.

[2] Swarts, Francis, CDMA techniques for third generation mobile systems, Kluwer Academic Publishers, 1999

[3] Yang, Samuel C., CDMA RF system engineering, Artech House, 1998

[4] G. E. Bottomley, T. Ottosson, and Y.-P. E. Wang, "A generalized rake receiver for interference suppression," IEEE J. Sel. Areas Commun., vol. 18, no. 8, pp. 1536–1545, Aug. 2000.

[5] Jonh G. Proakis, "Digital Communications", MGraw-Hill, 1989.

[6] Devroye, N.; Mitran, P.; Tarokh, V,"Achievable rates in cognitive radio channels", Information Theory, IEEE Transactions on, Volume 52, Issue 5, May 2006 Pag.1813 - 1827

[7] Agilent Technologies Application Note, "Circuit Envelope Simulation", August 2005.

[8] Aparin, V.; Larson, L.E., "Analysis and reduction of cross-modulation distortion in CDMA receivers" Microwave Theory and Techniques, IEEE Transactions on, Volume 51, Issue 5, May 2003 Page(s):1591 – 1602

[9] David middleton, "An Introduction To Statistical Communication Theory", IEEE Press, 1920

[10] I. S. REED, "on a Moment Theorem for complex Gaussian Processes", IRE Transactions On Information Theory, Volume 8, Issue 3, Apr 1962 Page(s):194 – 195

[11] K. G. Gard, H. M. Gutierrez, and M. B. Steer, "Characterization of spectral regrowth in microwave amplifiers based on the nonlinear transformation of a complex Gaussian process," IEEE Trans. Microwave Theory and Tech., vol. 47, 1999, pp. 1059-1069.

[12] Zhou, G.T, "Analysis of spectral regrowth of weakly nonlinear power amplifiers", IEEE Communications Letters, Volume 4, Issue 11, Nov. 2000 Page(s):357 – 359

[13] Aparin, V., "Analysis of CDMA signal spectral regrowth and waveform quality", IEEE Trans. Microwave Theory and Techniques, Vol. 49, Is. 12, pp. 2306 – 2314, Dec. 2001.

[14] David E. Reed and Mark A. Wickert, "Nonstationary of a random binary pulse train", IEEE Transactions On Information Theory, Vol. 35, no 3, May 1989.

[15] N. B. Carvalho and J. C. Pedro, "A Comprehensive Explanation of Distortion Sideband Asymmetries", IEEE Trans. on Microwave Theory and Tech., Vol. MTT-50, pp. 2090 – 2101, Sept. 2002,.

[16] H. C. Ku, M. D. McKinley, and J. S. Kenney, "Quantifying memory effects in RF power amplifiers," IEEE Trans. Microwave Theory & Tech., Vol. MTT-50, pp. 2843-2849, Dec. 2002

[17] J. C. Pedro and N. B. Carvalho, Intermodulation Distortion in Microwave and Wireless Circuits, Artech House, Inc., Norwood MA, 2003.

[18] J. P. Martins, Cabral P. M., N. B. Carvalho, and J. C. Pedro, "A Metric for the Quantification of Memory Effects in Power Amplifiers," IEEE Trans. on Microwave Theory and Tech., in press.

[19] Walker, A.; Steer, M.; Gard, K., "Capturing asymmetry in distortion of an RF system using a multi-slice behavioral model", IEEE Microwave and Wireless Components Letters, Vol. 16, Iss. 4, pp. 212 – 214, April 2006.

[20] J. P. Martins, N. B. Carvalho and J. C. Pedro, ”Multi-sine Response of Third Order Nonlinear Systems with Memory Based on Two-tone Measurements,” 36th European Microwave Conference, Manchester, Sept. 2006.

[21] Stephen O. Rice, “Envelopes of Narrow-Band Signals”, Proceedings of the IEEE, Vol 70, No 7, July 1982.

[22] J. F. Sevic and M. B. Steer, “On the significance of envelope peak-to-average ratio for estimating the spectral regrowth characteristics of an RF/Microwave power amplifier,” *IEEE Trans. Microwave Theory Techniques,* Vol. 48, June 2000, pp. 1068–1071.

[23] Krongold, B.S.; Jones, D.L., “PAR reduction in OFDM via active constellation extension”, IEEE Transactions on Broadcasting, Volume 49, Issue 3, Sept. 2003 Page(s):258 - 268

[24] Kwok, H.; Jones, D., “PAR reduction via constellation shaping,”Information Theory, 2000, IEEE International Symposium on Proceedings, 25-30 June 2000 Page(s):166

[25] Zhixing Yang; Haidong Fang; Changyong Pan “ACE with frame interleaving scheme to reduce peak-to-average power ratio in OFDM systems”, IEEE Transactions on Broadcasting ,Volume 51, Issue 4, Dec. 2005 Page(s):571 - 575

[26] Sezginer, S.; Sari, H., “OFDM peak power reduction with simple amplitude predistortion”, IEEE Communications Letters, Volume 10, Issue 2, Feb. 2006 Page(s):65 - 67

[27] J. Tellado-Mourelo, “Peak to average power reduction for multicarrier modulation,” Ph.D. dissertation, Stanford University, Sept. 1999.

[28] Chan-Soo Hwang, “Peak power reduction method for multicarrier transmission” Electronics Letters, Volume 37, Issue 17, 16 Aug. 2001 Page(s):1075 – 1077

[29] Seung Hee Han; Jae Hong Lee, "An overview of peak-to-average power ratio reduction techniques for multicarrier transmission", IEEE Wireless Communications, Volume 12, Issue 2, April 2005 Page(s):56 - 65

[30] Kwok, H.; Jones, D., "PAR reduction via constellation shaping", IEEE International Symposium on Information Theory, 2000, 25-30 June 2000 Page(s):166

[31] Kou, Y.; Wu-Sheng Lu; Antoniou, A., "New peak-to-average power-ratio reduction algorithms for multicarrier communications", IEEE Transactions on Circuits and Systems, Volume 51, Issue 9, Sept. 2004 Page(s):1790 - 1800

[32] Zhixing Yang; Haidong Fang; Changyong Pan, "ACE with frame interleaving scheme to reduce peak-to-average power ratio in OFDM systems", IEEE Transactions on Broadcasting, Volume 51, Issue 4, Dec. 2005 Page(s):571 - 575

[33] Ochiai, H.; Imai, H., "Performance of the deliberate clipping with adaptive symbol selection for strictly band-limited OFDM systems", IEEE Journal on Selected Areas in Communications, Volume 18, Issue 11, Nov. 2000 Page(s):2270 - 2277

[34] Guangliang Ren; Hui Zhang; Yilin Chang, "A complementary clipping transform technique for the reduction of peak-to-average power ratio of OFDM system", IEEE Transactions on Consumer Electronics, Volume 49, Issue 4, Nov. 2003 Page(s):922 - 926

[35] Tarokh, V.; Jafarkhani, H , "On the computation and reduction of the peak-to-average power ratio in multicarrier communications", , IEEE Transactions on Communications, Volume 48, Issue 1, Jan. 2000 Page(s):37 - 44

[36] Vaananen, O.; Vankka, J.; Viero, T.; Halonen, K , "Reducing the crest factor of a CDMA downlink signal by adding unused channelization codes", IEEE Communications Letters, Volume 6, Issue 10, Oct. 2002 Page(s):443 – 445

[37] Chow, J.S.; Bingham, J.A.C.; Flowers, M.S., "Mitigating clipping noise in multi-carrier systems", 1997. ICC 97 Montreal, IEEE International Conference on Communications 'Towards the Knowledge Millennium, Volume 2, 8-12 June 1997 Page(s):715 - 719 vol.2

[38] Raich, R.; Hua Qian; Zhou, G.T , "Optimization of SNDR for amplitude-limited nonlinearities", IEEE Transactions on Communications, Volume 53, Issue 11, Nov. 2005 Page(s):1964 - 1972

[39] Xiao Huang; Jianhua Lu; Junli Zheng; Chuang, J.; Jun Gu., "Reduction of peak-to-average power ratio of OFDM signals with companding transform", Electronics Letters,Volume 37, Issue 8, 12 Apr 2001 Page(s):506 - 507

[40] Vaananen, O.; Vankka, J.; Halonen, K., "Reducing the peak to average ratio of multicarrier GSM and edge signals", The 13th IEEE International Symposium on Personal, Indoor and Mobile Radio Communications, Volume 1, 15-18 Sept. 2002 Page(s):115 - 119 vol.1

[41] Tao Jiang; Guangxi Zhu., "Nonlinear companding transform for reducing peak-to-average power ratio of OFDM signals", IEEE Transactions on Broadcasting, Volume 50, Issue 3, Sept. 2004 Page(s):342 - 346

[42] Xiao Huang; Jianhua Lu; Junli Zheng; Letaief, K.B.; Jun Gu., "Companding transform for reduction in peak-to-average power ratio of OFDM signals", IEEE Transactions on Wireless Communications Volume 3, Issue 6, Nov. 2004 Page(s):2030 - 2039

[43] Pratt, T.G.; Jones, N.; Smee, L.; Torrey, M., "OFDM link performance with companding for PAPR reduction in the presence of non-linear amplification" IEEE Transactions on Broadcasting, Volume 52, Issue 2, June 2006 Page(s):261 - 267

[44] Khaled M. Gharaibeh, Kevin Gard and Michael Steer, "Accurate Estimation of Digital Communication System Metrics – SNR, EVM and ρ in a Nonlinear Amplifier Environment", ARTFG Microwave Measurements Conference 2004

[45] N.B. Carvalho and J. C. Pedro, "Compact Formulas To Relate ACPR and NPR To Two-Tone IMR and IP3" in Microwave Journal

[46] M.C. Jeruchim, P. Balaban, and K.S. Shanmugan. Simulation of Communication Systems: modeling methodology and techniques, Kluwer Academic, New York, 2000, 2^{nd} Ed.

[47] J. P. Martins, N. B. Carvalho and J. C. Pedro, "Co-channel and Adjacent Channel Distortion in Microwave Amplifiers Presenting Memory ", Submitted to the IEEE Transactions on MTT

[48] J. Bendat, Random Data: Analysis and Measurement Procedures, 3rd ed. New York: Wiley, 2000

[49] Lavrador, P.M.; de Carvalho, N.B.; Pedro, J.C.; "Evaluation of signal-to-noise and distortion ratio degradation in nonlinear systems", IEEE Trans. Microwave Theory and Techniques, Vol. 52, Is. 3, pp. 813 – 822, Mar. 2004.

[50] Vladimir Aprin, Linearization of CDMA Receiver Front-Ends, PhD Thesis, University of California, San Diego, 2005.

[51] H. C. Ku, M. D. McKinley, and J. S. Kenney, "Quantifying memory effects in RF power amplifiers," IEEE Trans. Microwave Theory & Tech., Vol. MTT-50, pp. 2843-2849, Dec. 2002

[52] Simulation and Model-Based design, Matlab tool

[53] Vector Signal Analyser 89600 Series, Agilent Technologies

[54] Pedro, J.C.; Borges de Carvalho, N.; "Evaluating co-channel Distortion Ratio in Microwave Power Amplifiers", IEEE Transactions on Microwave Theory and Techniques, Vol. 49, Is. 10, Part 1, pp. 1777 – 1784, Oct. 2001

[55] Ku, H., W. Woo, and J. S. Kenney, ''Carrier-to-Interference Ratio Prediction of Nonlinear RF Devices,'' Microwave Journal, Vol. 44, No. 2, pp. 154–164, 2001

[56] De Carvalho, N.B.; Pedro, J.C.;"Large- and Small-signal IMD Behaviour of Microwave Power Amplifiers", IEEE Transactions on Microwave Theory and Techniques, Vol. 47, Is. 12, pp. 2364 – 2374, Dec. 1999.

[57] J.C. Pedro and N. B. Carvalho, "Inferring Nonlinear Distortion Performance of Power Amplifiers Subject to Telecommunications Signals from Two-Tone Measurements", IEEE International Microwave Symposium, 2005

[58] Agilent Application Note 1335, "HPSK Spreading for 3G", 2000.

[59] How-Sian Yap, "Designing To Digital Wireless Specifcations Using Circuit Envelope Simulation", HP EEsof Division, Hewlett-Packard.

[60] Khaled M. Gharaibeh, Kevin Gard and Michael Steer, "Modeling and Measurement of Nonlinear Memory Effects in Wireless Communication Systems", IMS 2006 Presentation